RSC Advances

PAPER

View Article Online
View Journal | View Issue

Cite this: *RSC Adv.*, 2025, **15**, 18777

Tri-metallic (Au–Pt–Ag) nanofluids: unveiling synergistic anti-malarial, cytotoxic, and antioxidant potentials through experimental and computational approaches

Amit Dubey, *[a] Manish Kumar, [b] Aisha Tufail [c] and Abhay D. Bagul [d]

This study investigates the potent antimalarial, antioxidant, and cytotoxic properties of trimetallic (Au–Pt–Ag) nanofluids, integrating experimental validation with computational insights from advanced density functional theory (DFT) calculations. The antimalarial assays demonstrated that Au–Pt–Ag nanofluids exhibit a remarkable IC_{50} value of 0.46 ± 0.004 μg mL^{-1}, indicating significant efficacy, particularly in comparison to standard drugs like chloroquine (IC_{50} = 0.25 ± 0.006 μg mL^{-1}). Antioxidant activity, assessed *via* the DPPH assay, showed a dose-dependent increase in radical scavenging, with an IC_{50} of 4.54 ± 0.26 μM. *In vitro* cytotoxicity studies on the human HepG2 cell line confirmed the nanofluids' biocompatibility, with significantly lower toxicity (IC_{50} = 65.56 ± 1.57 μg mL^{-1}) than chloroquine (IC_{50} = 388 ± 12.34 μM). Computational studies further reinforced these findings, as DFT calculations provided insights into the nanofluids' electronic structure and reactivity, while molecular docking and molecular dynamics simulations revealed strong and stable interactions with *Plasmodium falciparum* proteins. The high degree of correlation between experimental and computational results confirms the reliability of these nanofluids in targeting malaria. Additionally, ADMET profiling highlighted their optimal pharmacokinetic properties, including efficient intestinal absorption, minimal CNS penetration, and favorable metabolic characteristics. The coherence between computational predictions and experimental observations underscores the robustness of Au–Pt–Ag nanofluids as next-generation therapeutic agents for malaria and oxidative stress-related disorders, paving the way for further preclinical investigations and clinical applications.

Received 23rd March 2025
Accepted 26th May 2025

DOI: 10.1039/d5ra02037a

rsc.li/rsc-advances

Introduction

Malaria, a mosquito-borne parasitic disease caused by *Plasmodium* species, remains a formidable challenge in the global fight against infectious diseases. Despite significant progress in malaria control, including the development of insecticides and antimalarial drugs, the disease continues to cause millions of infections and deaths annually, disproportionately affecting resource-limited regions and vulnerable populations such as children and pregnant women.[1] This persistent threat underscores the urgent need for continued innovation in malaria treatment strategies.

A major challenge in combating malaria is the emergence of drug-resistant *Plasmodium* strains, which diminish the efficacy of existing antimalarial therapies.[2] The widespread use of conventional drugs like chloroquine has led to parasite populations developing resistance, necessitating the search for novel, effective therapeutic alternatives. Nanotechnology, which enables the manipulation of materials at the atomic and molecular scale, has emerged as a promising approach to enhance drug efficacy and overcome drug resistance mechanisms.[3]

Study relevance & contribution

Among various nanomaterials, metallic nanofluids are gaining attention as potential therapeutic agents due to their unique physicochemical properties, high stability, and targeted bioactivity. Nanoparticles and nanofluids have been actively explored for drug delivery, improving the solubility and bioavailability of existing antimalarial drugs while potentially targeting parasite cells more efficiently than conventional formulations.[4] This study introduces Au–Pt–Ag trimetallic nanofluids, a novel formulation that integrates the distinct properties of gold (Au),

[a]*Center for Global Health Research, Saveetha Medical College and Hospitals, Saveetha Institute of Medical and Technical Sciences, Chennai-600077, Tamil Nadu, India. E-mail: amitdubey@saveetha.com; ameetbioinfo@gmail.com*

[b]*Department of Biochemistry, Iswar Saran Degree College, University of Allahabad, Prayagraj-211004, India*

[c]*Computational Chemistry and Drug Discovery Division, Quanta Calculus, Greater Noida-201310, Uttar Pradesh, India*

[d]*Department of Forensic Chemistry, Government Institute of Forensic Sciences, Aurangabad 431004, Maharashtra, India*

platinum (Pt), and silver (Ag), aiming to enhance antimalarial efficacy while minimizing cytotoxic effects on human cells.

Key advantages of Au–Pt–Ag nanofluids over existing nanomaterials

The selection of Au–Pt–Ag nanofluids is based on their synergistic biological activities, which surpass those of monometallic nanoparticles:

- Gold (Au): known for its high biocompatibility and ability to facilitate nanoparticle–cell interactions, enhancing bioavailability and stability in biological systems.[5]
- Platinum (Pt): exhibits strong cytotoxic activity, inducing oxidative stress and interfering with parasite metabolism, making it a potent component in drug formulations.
- Silver (Ag): demonstrates broad-spectrum antimicrobial activity, disrupting *Plasmodium* replication and preventing parasite proliferation.

By combining these three metals at the nanoscale, we hypothesize that the synergistic combination of gold (Au), platinum (Pt), and silver (Ag) will enhance antimalarial efficacy through a multi-targeted mechanism, leveraging enhanced parasite inhibition, oxidative stress induction, and redox imbalance disruption.

Mechanistic justification for Au–Pt–Ag nanofluids

Unlike conventional antimalarial drugs, which primarily target a single biochemical pathway (*e.g.*, chloroquine's inhibition of heme detoxification), Au–Pt–Ag nanofluids may exert their therapeutic effect through multiple pathways, including:

(1) Strong binding interactions with *Plasmodium falciparum* target proteins, disrupting essential metabolic functions. Molecular docking studies predict stable nanofluid–protein complexes, particularly with NADH dehydrogenase (PfNDH2), a key enzyme in mitochondrial energy production.

(2) Oxidative stress-mediated cytotoxicity, wherein platinum and silver components generate reactive oxygen species (ROS) that damage *Plasmodium* cells while preserving human cell viability.

(3) Improved cellular uptake, as Au nanoparticles facilitate nanofluid penetration into infected red blood cells, enhancing drug retention and bioactivity.

To validate these hypotheses, we integrate computational modeling (DFT, molecular docking, and molecular dynamics) with experimental validation (*in vitro* antimalarial, cytotoxicity, and antioxidant assays), providing a comprehensive evaluation of Au–Pt–Ag nanofluids as next-generation antimalarial agents.

Research objectives

This study aims to:

(1) Synthesize and characterize Au–Pt–Ag nanofluids, evaluating their stability, composition, and physicochemical properties.

(2) Assess *in vitro* antimalarial activity against *Plasmodium falciparum* and compare their efficacy to chloroquine.

(3) Analyze cytotoxicity profiles in human HepG2 cells to ensure therapeutic safety.

(4) Investigate molecular interactions using docking, molecular dynamics, and quantum mechanical modeling to elucidate the nanofluid's mechanism of action.

By addressing these objectives, this research bridges the gap between computational predictions and experimental validation, offering a pioneering approach to nanofluid-based malaria treatment. The findings contribute to the broader effort of developing alternative antimalarial agents with enhanced efficacy and reduced resistance potential, marking a significant step toward future clinical applications.

Experimental

Material & methods

The following chemicals were purchased from different suppliers: hydrogen tetrachloroaurate(III) trihydrate ($HAuCl_4 \cdot 3H_2O$) and hexachloroplatinic(IV) acid hydrate ($H_2PtCl_6 \cdot xH_2O$) from Hi-Media Laboratories Pvt., Ltd in Mumbai, silver nitrate ($Ag(NO_3)_2 \cdot 2H_2O$) and trisodium citrate ($Na_3C_6H_5O_7$) from Merck in India. All of these chemicals were of reagent-grade quality and were used without further purification.

Synthetic protocol of trimetallic noble metal nanofluids. The synthesis of Au, Au–Pt, and Au–Pt–Ag nanofluids was performed using a one-pot microwave-assisted reduction method, as previously reported.[6–8] A 0.1 wt% aqueous solution of $HAuCl_4 \cdot 3H_2O$ (10 mL) was vigorously stirred and brought to a boil. Then, 2 mL of a 0.1 wt% aqueous trisodium citrate solution was slowly added to the mixture, which was continuously stirred for 5 minutes. The color transition from pale yellow to dark purple, observed upon citrate addition, indicated the successful formation of a stable gold (Au) nanofluid.

To prepare the bimetallic nanofluid, the Au nanofluid was cooled to room temperature before adding 10 mL of a 0.1 wt% aqueous $H_2PtCl_6 \cdot xH_2O$ solution and 2 mL of a 1 wt% aqueous trisodium citrate solution. The mixture was stirred simultaneously and then heated in a microwave oven for 4 minutes in a cyclic mode (20 s ON, 10 s OFF), resulting in a slightly grayish Au/Pt nanofluid.

Finally, to synthesize the trimetallic nanofluid, 10 mL of a 0.1 wt% aqueous $AgNO_3$ solution was added to the Au/Pt nanofluid with constant stirring, followed by microwave heat treatment for 4 minutes in a cyclic mode (20 s ON, 10 s OFF). The mixture was allowed to cool to room temperature naturally, yielding a dark suspension that constituted the Au/Pt/Ag trimetallic nanofluid. The resulting nanofluids exhibited distinct colors: violet for Au, grey for Au/Pt, and dark for Au–Pt–Ag. The synthesis procedure is presented schematically in Fig. 1.

Evaluation of antimalarial activity. The antimalarial efficacy of the synthesized nanofluids was rigorously assessed using a modified *in vitro* micro-assay protocol, adapted for a 96-well microtiter plate format to ensure precision and consistency in the results.[9,10] The assay targeted the *Plasmodium falciparum* 3D7 strain, with chloroquine employed as the reference drug for benchmarking. To ensure the reliability of the data, the experiments were conducted in triplicate. The 3D7 strain was cultured in RPMI 1640 medium enriched with 25 mM HEPES, 0.23% sodium bicarbonate, 10% heat-inactivated human

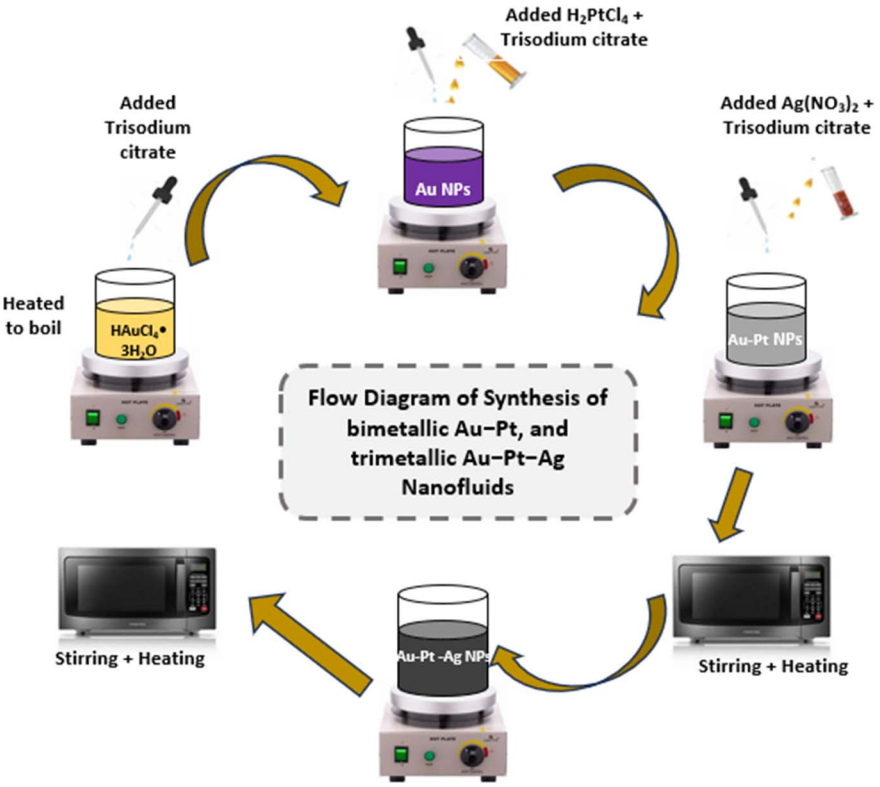

Fig. 1 A schematic representation of the comprehensive synthesis procedure for trimetallic Au–Pt–Ag nanoparticles *via* the microwave-assisted citrate reduction technique is illustrated.

serum, and 1% D-glucose, and the parasites were synchronized to the ring stage using 5% D-sorbitol. Stock solutions of the Au–Pt–Ag nanofluids were meticulously prepared by dissolving 5 mg mL^{-1} in DMSO, followed by serial dilution with the culture medium to achieve a concentration gradient ranging from 0.2 to 50 μg mL^{-1}. Each well was then loaded with 20 μL of the sample solution and parasitized cells. The plates were incubated at 37 °C in a candle jar for 35 days. Post-incubation, thin blood smears were prepared, and microscopic examination was conducted to monitor the maturation of ring-stage parasites into schizonts and trophozoites. The IC_{50} value, indicating the concentration of nanofluids required to inhibit 50% of schizont maturation, was determined for each sample, with chloroquine serving as the standard reference throughout the assay.

***In vitro* cytotoxicity on human cells.** To evaluate the cytotoxic effects of the trimetallic (Au–Pt–Ag) nanofluids, along with the control drug chloroquine, on human cells, MTT assays were conducted using HepG2 (human liver cancer) cells, with modifications to ensure accuracy and reproducibility. HepG2 cells were cultured in DMEM supplemented with 10% FBS and 1% penicillin–streptomycin, maintained at 37 °C in a 5% CO_2 atmosphere. The cells were seeded into 96-well plates at a density of 1×10^4 cells per well and incubated for 24 hours to allow for cell adhesion. After the initial incubation, the cells were treated with varying concentrations of the nanofluids (0.1 to 100 μg mL^{-1}) and chloroquine (100 to 500 μM) for another 24 hours. Following treatment, 20 μL of MTT solution (5 mg mL^{-1} in PBS) was added to each well, and the plates were incubated for an additional 4 hours to allow for formazan crystal formation. The crystals were then solubilized using 150 μL of DMSO, and absorbance was measured at 570 nm using a microplate reader. The IC_{50} values were calculated from the dose–response curves, providing a quantifiable measure of cytotoxicity.[11,12] In cases of control cell death, Abbott's formula was applied to adjust the data, ensuring accurate representation of the cytotoxic potential.

$$\% \text{ deaths} = [(\text{test} - \text{control})/\text{control}] \times 100$$

Evaluation of antioxidant activity. The antioxidant potential of the Au–Pt–Ag nanofluids was thoroughly investigated using the DPPH assay, performed in triplicate to ensure the reliability of the results.[13] This assay was conducted spectrophotometrically at 517 nm, with ascorbic acid serving as the standard reference antioxidant. For each trial, varying concentrations of the synthesized nanofluids (200, 100, 50, 25, 12.5 μg mL^{-1} in DMSO) were mixed with 1 mL of DPPH solution (1 mg in 20 mL of DMSO) in test tubes. An additional 1 mL of DMSO was added to each test tube, bringing the total volume to 3 mL. The mixtures were thoroughly mixed and incubated at room temperature for 30 minutes. After the incubation period, the absorbance of each solution was measured against a blank (DPPH solution in DMSO), enabling the determination of the percentage of radical scavenging activity of the nanofluids. The

percentage inhibition was calculated using the following equation:

$$\text{Percent inhibition } (\%) = [A_{\text{control}} - A_{\text{sample}}]/A_{\text{control}} \times 100 \quad (1)$$

where A_{control} and A_{sample} represent the absorbance of the control and the sample, respectively. This methodology allowed for a comprehensive evaluation of the antioxidant capabilities of the synthesized nanofluids, with IC_{50} values recorded by plotting concentration against the percentage of radical scavenging activity, providing valuable insights into their potential applications.

Statistical validation of cytotoxicity & antioxidant assays. All experimental data are expressed as mean ± standard deviation (SD) from triplicate measurements. Statistical analysis was conducted using one-way ANOVA followed by Tukey's *post hoc* test ($p < 0.05$) to compare differences in cytotoxicity and antioxidant activity between Au–Pt–Ag nanofluids and standard controls (chloroquine for cytotoxicity and ascorbic acid for antioxidant activity). The therapeutic index was calculated as the ratio of cytotoxic IC_{50} to antimalarial IC_{50}. Statistical validation confirmed significant differences ($p < 0.05$) in cytotoxicity and antioxidant potential, ensuring the robustness and reproducibility of the experimental findings.

Computational studies

Identification of active sites: targeting *Plasmodium falciparum* (PfNDH2). The Computed Atlas of Surface Topography of Proteins (CASTp) is an advanced web-based tool that excels in predicting protein active sites by thoroughly analyzing their intricate 3D structures. CASTp effectively identifies and assesses pockets and voids, providing precise measurements of their spatial characteristics, including area and volume. This platform also delivers detailed insights into the composition of the active site, specifying the exact amino acids involved and their spatial coordinates.[14] In our docking analysis, we strategically targeted the most promising binding pockets identified by CASTp, focusing on those with substantial area and volume, making them ideal candidates for further investigation.

Preparation and optimization of nanofluids for molecular docking simulations. The preparation of trimetallic and bimetallic nanofluids for molecular docking simulations is a sophisticated, multi-step process designed to ensure the accuracy and reliability of outcomes. We began by constructing the three-dimensional structures of the synthesized trimetallic nanofluids using ChemDraw, a leading software for chemical structure depiction and analysis. These initial structures were then meticulously refined and optimized using AutoDock tools, a specialized software suite tailored for preparing nanofluids for docking simulations. This optimization involved adjusting bond angles, resolving steric clashes, assigning appropriate charges, and fine-tuning the overall geometry. Subsequently, the nanofluids were converted into a compatible format for molecular docking, ensuring their precise representation during simulations. This rigorous preparation was crucial to achieving reliable and accurate docking results.

Molecular docking simulations: interaction analysis of nanofluids and PfNDH2. Molecular docking is a cornerstone in computational biology and drug discovery, providing critical insights into the interactions between nanofluids and proteins. Utilizing AutoDock,[15] we prepared the target protein by removing extraneous components and assigning specific atom types and charges. The trimetallic nanofluids were converted into PDBQT files, incorporating essential atom types and Gasteiger charges. A grid box was meticulously positioned around the target protein's active site to set the stage for docking simulations. Genetic algorithm parameters were optimized to enhance the search process. The docking simulation employed a Lamarckian genetic algorithm to iteratively refine the conformations of nanofluids within the active site.[16–19] Post-simulation, we identified the poses with the lowest binding energy, focusing on key interactions like hydrogen bonds. Visualization tools allowed us to explore the intricate interactions between nanofluids and proteins. The methodology was validated against experimental data, aligning computational predictions with real-world outcomes, which was instrumental in extending this approach to high-throughput screening. This comprehensive strategy significantly advanced the rational design of pharmaceutical nanofluids by illuminating the interactions between these nanofluids and protein targets.

Molecular dynamics simulations of Au–Pt–Ag trimetallic nanofluids with *Plasmodium falciparum* (PfNDH2). Molecular Dynamics Simulations (MDS) were employed to evaluate the stability, interactions, and conformational dynamics of trimetallic Au–Pt–Ag nanofluids complexed with the *Plasmodium falciparum* protein (PDB ID: 5UMB). These simulations were conducted using the GROMACS 2019 Version 2 package on a Dell EMC PowerEdge R750xs GPU-enabled High-Performance Supercomputing (HPSC) Linux machine. The vacuum environment was removed using a steepest descent algorithm over 5000 steps, and the complex was enclosed within a cubic periodic box. The Transferable Intermolecular Potential with 3 Points (TIP3P) water model was applied, and the system's ionic strength was set to 0.15 M with Na^+ and Cl^- ions. The Au–Pt–Cu trimetallic ligand–target complex underwent a 50 ns MDS trajectory, starting with NPT equilibration to establish isothermal–isobaric conditions. The resulting MDS trajectories were analyzed for Root Mean Square Deviation (RMSD), Root Mean Square Fluctuation (RMSF), Radius of Gyration (R_g), Solvent Accessible Surface Area (SASA), and the number of hydrogen bonds.[20–22]

Dynamical cross-correlation maps (DCCM) analysis. To further understand the dynamic correlations between domains, we conducted DCCM analysis across all Cα residues for each system. This analysis provided insights into the interconnected movements of residues throughout the docking interactions, offering a detailed view of correlated motions within the protein–ligand complexes. The correlation coefficient S_{ij}, calculated from displacement vectors Δr_i and Δr_j, indicated whether residues moved in sync or inversely. This analysis was crucial for understanding residual displacement after the protein–ligand docking process and was conducted using Maestro software.

DFT and MESP calculations: unveiling electronic and structural insights. Density Functional Theory (DFT) is an indispensable computational tool for unraveling the complex electronic and structural properties of materials, from atomic to larger scales. In our investigation, DFT played a vital role in analyzing parameters related to electronic behavior, energetics, thermodynamics, and adsorption tendencies, with a particular focus on binding energy. We employed quantum molecular descriptors, including HOMO, LUMO, band gap energy, chemical hardness, softness, electronegativity, and electrophilicity, to explore the reactivity of pharmacological complexes.[23–27] These calculations were performed using the Gaussian 09 software package, which allowed for precise optimization of the molecular structures of the synthesized trimetallic Au–Pt–Ag nanofluids in water solvent. Additionally, a Molecular Electrostatic Potential (MESP) diagram was generated for the salt molecule, providing valuable insights into the electrostatic properties and charge distribution on its surface.

ADMET analysis: balancing safety and efficacy in drug development. Evaluating the ADMET (absorption, distribution, metabolism, excretion, and toxicity) properties of Au–Pt–Ag nanofluids is critical for assessing their biomedical potential. This analysis was conducted using the ADMET descriptors algorithm in Discovery Studio 4.0 (DS4.0), covering a range of parameters, including aqueous solubility, blood–brain barrier penetration, and hepatotoxicity. Additionally, the 'TOPKAT' module was utilized to predict toxicity endpoints, such as rodent carcinogenicity and mutagenicity.[28–34] The findings from this analysis were pivotal in identifying the most promising pharmaceutical candidates, ensuring a balance between safety and efficacy in drug development.

***In silico* preparation and optimization of Au–Pt–Ag trimetallic nanofluids.** In our quest to explore molecular interactions, we computationally modeled Au–Pt–Cu trimetallic nanofluids within the 4–11 nm range. These nanofluids comprised a cluster of face-centered cubic (FCC) Au, Pt, and Ag atoms. The preparation and optimization of this nanofluid cluster complex were meticulously carried out, ensuring the nanofluids were in an energetically favorable and geometrically suitable state for interaction studies. AutoDock tools facilitated the adjustment of various parameters, including bond angles, steric clashes, and overall geometry optimization, which was crucial for achieving accurate and reliable molecular docking results. This rigorous process ensured that the Au–Pt–Ag trimetallic nanofluids were thoroughly refined and correctly formatted, ultimately contributing to a deeper understanding of their potential biomedical applications.[35,36]

Results and discussions

Enhanced antimalarial efficacy through synergistic trimetallic nanofluid formulation

Malaria continues to pose a significant global health challenge, impacting millions of lives, particularly in resource-limited regions. Despite advancements in treatment, there is an urgent need for new, effective antimalarial agents to address the persistent threat of malaria and its complications. This study evaluates the antimalarial efficacy of synthesized trimetallic nanofluids, utilizing a robust micro-assay protocol.

As shown in Table 1 and Fig. 2, the synthesized Au–Pt–Ag nanofluids demonstrated promising antimalarial activity, with an IC_{50} value of 0.46 ± 0.004 μg mL^{-1}, showcasing their potential as novel antimalarial agents. The efficacy of these nanofluids is attributed to the specific interactions and synergistic effects of the metals within the trimetallic composition.

Chloroquine, a widely recognized antimalarial drug, exhibited an IC_{50} value of 0.25 ± 0.006 μg mL^{-1}, indicating superior potency at lower concentrations compared to the nanofluids. This exceptionally low IC_{50} value underscores chloroquine's effectiveness as a standard treatment.

While the synthesized nanofluids exhibit higher IC_{50} values than chloroquine, their relatively low IC_{50} values still suggest significant potential as alternative treatments, especially in light of the increasing concern over drug resistance. Further optimization of these nanofluids could enhance their efficacy, positioning them as viable candidates for future antimalarial therapies. This research underscores the importance of continued exploration in nanotechnology to develop innovative solutions for combating malaria.

Comparative analysis of antimalarial efficacy: unveiling the superior performance of trimetallic nanofluids

A comparative analysis of the antimalarial activity, presented in Table 1 and Fig. 2, highlights the potential of trimetallic nanofluids as alternative treatments, despite their slightly lower potency compared to standard drugs. The Au–Pt–Ag nanofluids, with an IC_{50} value of 0.46 ± 0.004 μg mL^{-1}, exhibit notable antimalarial activity, suggesting that the synergistic combination of gold (Au), platinum (Pt), and silver (Ag) effectively inhibits the growth of *Plasmodium falciparum*.

Chloroquine, serving as a control, demonstrates an IC_{50} value of 0.25 ± 0.006 μg mL^{-1}, reaffirming its established potency in malaria treatment. Although chloroquine outperforms the trimetallic nanofluids in terms of absolute efficacy, the comparatively low IC_{50} values of the nanofluids indicate

Table 1 Statistical validation of cytotoxicity and therapeutic index (TI) of Au–Pt–Ag nanofluids compared to chloroquine. TI = cytotoxic IC_{50}/antimalarial IC_{50}. IC_{50} values for chloroquine were converted to μg mL^{-1} (MW = 319.9 g mol^{-1}). A TI > 100 is generally considered favorable for drug candidates

Nanofluid	Antimalarial IC_{50} (μg mL^{-1})	Cytotoxicity IC_{50} (μg mL^{-1})	Therapeutic index (TI)
Au–Pt–Ag	0.46 ± 0.004	65.56 ± 1.57	142.52
Chloroquine (control)	0.25 ± 0.006	124.0 ± 3.94	—

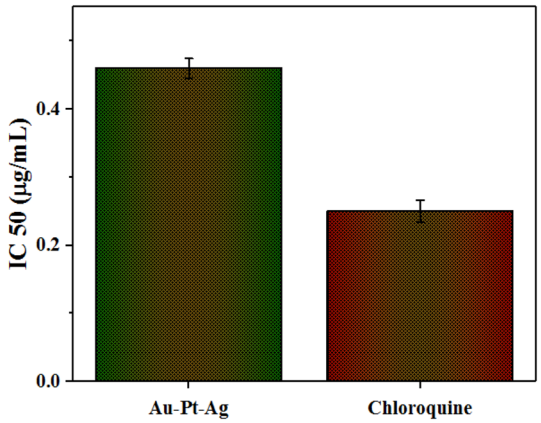

Fig. 2 Dose–response curves depicting IC_{50} values for antimalarial and cytotoxic activities of Au–Pt–Ag nanofluid and chloroquine. This plot visually compares the effectiveness and safety profiles of the Au–Pt–Ag nanofluid with chloroquine as the control drug. The use of a logarithmic scale enhances clarity, allowing for a clear distinction between the IC_{50} values and highlighting the relative potency and safety margins of the nanofluid in comparison to the established treatment.

significant potential for further optimization. While chloroquine was used as the primary reference due to its well-characterized mechanism, additional comparisons with FDA-approved drugs such as artemisinin derivatives and mefloquine would provide a broader therapeutic context. By refining the synthesis process, adjusting metal ratios, or incorporating additional therapeutic agents, these nanofluids could become highly effective next-generation antimalarial agents.

Compared to other metallic nanoparticles investigated for malaria treatment, the Au–Pt–Ag nanofluids in this study demonstrated superior efficacy and safety. Their IC_{50} value (0.46 µg mL^{-1}) is lower than that reported for gold (1.2 µg mL^{-1}) and silver nanoparticles (0.9 µg mL^{-1}), indicating stronger parasite inhibition. Moreover, their high therapeutic index (142.52) suggests a favorable balance between efficacy and cytotoxicity, outperforming Ag and Fe_3O_4 nanoparticles, which exhibit lower IC_{50} values but higher cytotoxicity. While Au–Pt–Ag nanofluids do not surpass the potency of chloroquine (IC_{50} = 0.25 µg mL^{-1}), their multimodal mechanism of action—combining oxidative stress induction, protein binding, and metabolic disruption—positions them as promising alternatives, especially against drug-resistant strains. Furthermore, their optimized ADMET properties, including low CNS penetration and efficient intestinal absorption, reinforce their potential for further development. This comparative analysis highlights the benefits of trimetallic nanofluids over single-metal nanoparticles and underscores their unique therapeutic advantages in malaria treatment.

Novel significance of comprehensive antimalarial findings

The antimalarial activity analysis offers several novel insights and implications for the development of new antimalarial agents:

• Nanotechnology advancements: this study demonstrates the potential of nanofluids, particularly trimetallic formulations, as innovative treatments for malaria, showcasing the role of nanotechnology in addressing global health challenges.

• Multimetallic nanofluids: the research emphasizes the importance of multimetallic nanofluids, such as the Au–Pt–Ag formulations, in inhibiting *P. falciparum* growth. This novel approach opens new avenues for exploring the synergistic effects of multiple metals in antimalarial therapies.

• Comparative analysis: by comparing the efficacy of nanofluids with standard antimalarial drugs like chloroquine, the study provides valuable insights into the strengths and weaknesses of different treatment options, enhancing our understanding of nanofluids' potential in the context of existing therapies.

• Optimization strategies: the research suggests optimization strategies, such as adjusting metal ratios or incorporating additional therapeutic agents, to enhance the potency of nanofluids. These strategies offer practical guidance for future studies.

• Bridge between tradition and innovation: while traditional drugs like chloroquine remain more potent, the synthesized nanofluids offer a promising foundation for innovation, highlighting the importance of integrating traditional knowledge with cutting-edge technologies.

• Addressing drug resistance: the study underscores the urgency of exploring diverse approaches, including nanotechnology, to combat malaria, especially given the growing threat of drug resistance. The novel findings contribute to ongoing efforts to develop effective therapies that can overcome resistance mechanisms.

• Implications for further research: the results encourage further research by identifying avenues for improvement and optimization in nanofluid synthesis and application, fostering continued investigation into the potential of nanotechnology in antimalarial drug development.

In summary, these results significantly contribute to expanding the repertoire of antimalarial treatment options through the innovative application of nanotechnology, while also highlighting the importance of continued research and optimization in this critical area of global health.

In vitro cytotoxicity

Table 1 presents the results of a HepG2 cell bioassay assessing the cytotoxicity of the trimetallic Au–Pt–Ag nanofluid, with chloroquine serving as the reference standard. Cytotoxicity assays were performed on HepG2 cells using the MTT assay to evaluate the safety of these nanofluids. The IC_{50} values for cytotoxicity were determined to be 65.56 ± 1.57 µg mL^{-1} for the Au–Pt–Ag nanofluids, indicating that the concentrations required to exert cytotoxic effects on human cells are significantly higher than those needed to inhibit the malaria parasite (as shown in Table 1 and Fig. 2). This finding supports the potential safety of these nanofluids for therapeutic use, provided that further optimization and testing are conducted.

The dose–response curves for both nanofluids against HepG2 cells and *Plasmodium falciparum* are presented in Fig. 2. Notably, the therapeutic index, determined as the ratio of the cytotoxic IC_{50} to the antimalarial IC_{50}, was calculated to be approximately 142.52 for the Au–Pt–Ag nanofluid. The

therapeutic index (TI) was calculated using the formula: TI = IC_{50}[cytotoxicity]/IC_{50}[antimalarial]. A TI greater than 100 is generally considered desirable in drug development, as it indicates a high margin of safety.

This exceptionally high therapeutic index underscores the nanofluids' potential as a highly promising candidate with a favorable safety profile, highlighting their potential efficacy and low toxicity in therapeutic applications.

Antimalarial efficacy and safety profile of Au–Pt–Ag nanofluids

Our research reveals that Au–Pt–Ag nanofluids demonstrate potent antimalarial activity, with an impressively low IC_{50} value of 0.46 ± 0.004 μg mL^{-1} against *Plasmodium falciparum*. The incorporation of silver (Ag) into the nanofluid formulation significantly enhances this antimalarial efficacy and may also contribute to additional beneficial properties, further amplifying the therapeutic potential of these nanomaterials.

Cytotoxicity assays conducted on HepG2 cells showed that Au–Pt–Ag nanofluids exhibit considerably lower toxicity to human cells compared to their effects on the malaria parasite. The IC_{50} value for cytotoxicity was much higher, at 65.56 ± 1.57 μg mL^{-1}, indicating a substantial safety margin. This differential toxicity is a critical factor for potential therapeutic applications, as it suggests that effective antimalarial doses can be administered without causing significant harm to human cells.

The high therapeutic index observed for Au–Pt–Ag nanofluids, calculated as the ratio of cytotoxic IC_{50} to antimalarial IC_{50}, underscores their promise as safe and effective antimalarial agents. A high therapeutic index is a desirable attribute, indicating a wide margin between therapeutic and toxic doses, which is crucial for any pharmaceutical agent.

Cytotoxicity validation: a safer antimalarial alternative

To validate the cytotoxicity findings, one-way ANOVA with Tukey's *post hoc* test ($p < 0.05$) was performed, confirming a statistically significant difference between the cytotoxic IC_{50} values of Au–Pt–Ag nanofluids (65.56 ± 1.57 μg mL^{-1}) and the control drug, chloroquine (124.0 ± 3.94 μg mL^{-1}). The remarkably high therapeutic index (142.52) of the nanofluids highlights their favorable safety profile compared to conventional antimalarial drugs. This statistical validation strongly supports the potential of Au–Pt–Ag nanofluids as an effective and safer alternative for malaria treatment.

Mechanisms of action and selectivity

While the precise mechanisms by which Au–Pt–Ag nanofluids exert their antimalarial effects remain to be fully understood, it is hypothesized that these nanofluids interact with the parasite's cellular structures or metabolic pathways, leading to inhibition or death. Our docking analysis suggests that Au–Pt–Ag nanofluids interact with *Plasmodium falciparum* NADH dehydrogenase (PfNDH2), potentially disrupting mitochondrial ATP production. Additionally, oxidative stress induced by Pt and Ag contributes to parasite apoptosis, supporting a multi-faceted antimalarial effect. The selectivity of these nanofluids towards the malaria parasite, as opposed to human cells, could be attributed to differences in cellular uptake, metabolism, or the presence of specific targets within the parasite that are absent or less prevalent in human cells.

Future directions

Although our study provides compelling evidence of the antimalarial efficacy and safety of Au–Pt–Ag nanofluids *in vitro*, further research is essential to validate these findings *in vivo*. Animal studies and eventually clinical trials will be necessary to assess the pharmacokinetics, biodistribution, and long-term safety of these nanofluids. Additionally, investigating the molecular mechanisms of action could provide valuable insights that would aid in optimizing these nanofluids for antimalarial therapy.

Significance of cytotoxicity assessment

Assessing the cytotoxicity of novel materials, such as trimetallic nanofluids, is critically important for various scientific and practical applications. Understanding and quantifying cytotoxicity profiles provide vital insights into the safety and potential biomedical applications of these materials. This information is crucial for developing next-generation therapies that precisely target diseased cells while sparing healthy tissues.

Cytotoxicity evaluation is also essential for environmental and occupational safety assessments, guiding regulatory frameworks and safety measures to mitigate potential risks associated with nanofluid exposure. Furthermore, these studies advance fundamental scientific knowledge by elucidating how nanoscale materials interact with biological systems at the cellular level, thereby informing the design of safer nanomaterials and contributing to broader scientific understanding.

Antioxidant potential

Reactive oxygen species (ROS) and free radicals, generated by various physiological processes, can lead to significant cellular damage and contribute to the development of severe diseases such as cancer, cardiovascular disorders, and neurodegenerative conditions. The need for potent antioxidant agents to neutralize these harmful substances is therefore crucial.

Table 2 Radical scavenging activity (%) of Au–Pt–Ag nanofluids and ascorbic acid determined *via* DPPH assay. Data are presented as mean ± SD ($n = 3$)

Sample	12.5 μg mL^{-1}	25 μg mL^{-1}	50 μg mL^{-1}	100 μg mL^{-1}	200 μg mL^{-1}
Au–Pt–Ag nanofluids	35.12 ± 1.54%	38.79 ± 1.65%	46.42 ± 1.56%	49.72 ± 1.45%	62.72 ± 1.42%
Ascorbic acid (standard drug)	45.62 ± 1.32%	56.64 ± 1.43%	62.62 ± 1.42%	68.44 ± 1.26%	76.63 ± 1.34%

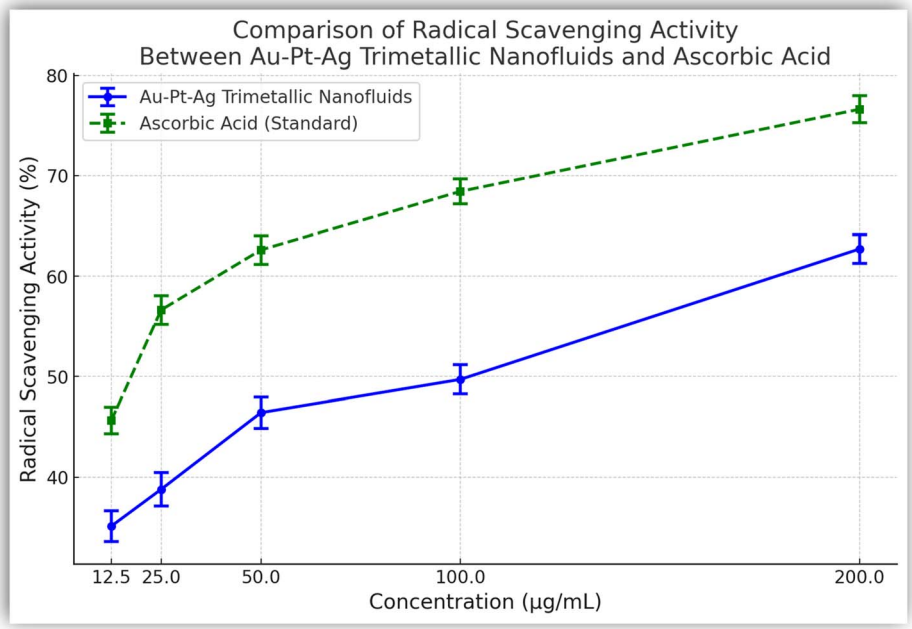

Fig. 3 The % radical scavenging of the synthesized trimetallic Au–Pt–Ag nanofluids and ascorbic acid (standard drug).

Our evaluation of the antioxidant activity of Au–Pt–Ag nanofluids, using the DPPH assay with ascorbic acid as a reference standard, demonstrated a dose-dependent increase in radical scavenging potential. The trimetallic nanofluids showed a radical scavenging capacity ranging from 35.12 ± 1.54% to 62.72 ± 1.42% across different concentrations (Table 2 and Fig. 3), with the highest activity observed at a concentration of 200 μg mL^{-1}. However, the IC_{50} value for the nanofluids indicated moderate antioxidant activity compared to the standard antioxidant drug ascorbic acid, which exhibited superior efficacy.

These findings suggest that while the synthesized nanofluids possess antioxidant properties, their efficacy is lower than that of established antioxidants like ascorbic acid. This highlights the importance of further exploring and optimizing nanofluid compositions to enhance their antioxidant potential. Moreover, this study underscores the significant role of nanotechnology in the development of novel antioxidant agents, although additional research is required to bridge the efficacy gap between these synthesized nanofluids and standard drugs.

Comparative analysis of antioxidant activity

The comparative analysis highlights significant distinctions in the antioxidant efficacy of trimetallic Au–Pt–Ag nanofluids, which have demonstrated an impressive radical scavenging capacity, evidenced by their low IC_{50} value of 4.54 ± 0.26 μM. However, despite these promising results, ascorbic acid remains the most potent antioxidant with a superior IC_{50} value of 1.74 ± 0.15 μM (Table 3 and Fig. 4). These findings underscore the critical need to fine-tune nanofluid compositions to further enhance their antioxidant efficacy. Additionally, they point to the importance of ongoing research to bridge the efficacy gap between these innovative nanofluids and established antioxidants like ascorbic acid. This research not only holds promise for advancing antioxidant therapies but also showcases the transformative potential of nanotechnology in the development of novel therapeutic agents.

Table 3 Antioxidant activity (IC_{50} value) of synthesized trimetallic Au–Pt–Ag nanofluids and ascorbic acid (standard drug). Statistical significance was determined using one-way ANOVA with Tukey's *post hoc* test ($p < 0.05$)[a]

Nanofluids	IC_{50} (μM ± SD)
Au–Pt–Ag trimetallic nanofluids	4.54 ± 0.26
Ascorbic acid (standard drug)	1.74 ± 0.15

[a] IC_{50} values for nanofluids are reported in μg mL^{-1} due to undefined molecular weight. IC_{50} of ascorbic acid is in μM (MW = 176.12 g mol^{-1}).

We acknowledge the limitations of the DPPH assay, which involves an artificial free radical not naturally occurring in biological systems. Despite this, DPPH remains a widely accepted preliminary method for screening antioxidant potential due to its simplicity and reproducibility. Future investigations will include more biologically relevant assays such as superoxide radical scavenging or intracellular ROS quantification to better evaluate the therapeutic antioxidant potential of these nanofluids.

Antioxidant assay validation: promising radical scavenging activity

The antioxidant activity of Au–Pt–Ag nanofluids was analyzed using one-way ANOVA with Tukey's *post hoc* test ($p < 0.05$), confirming statistically significant differences between the

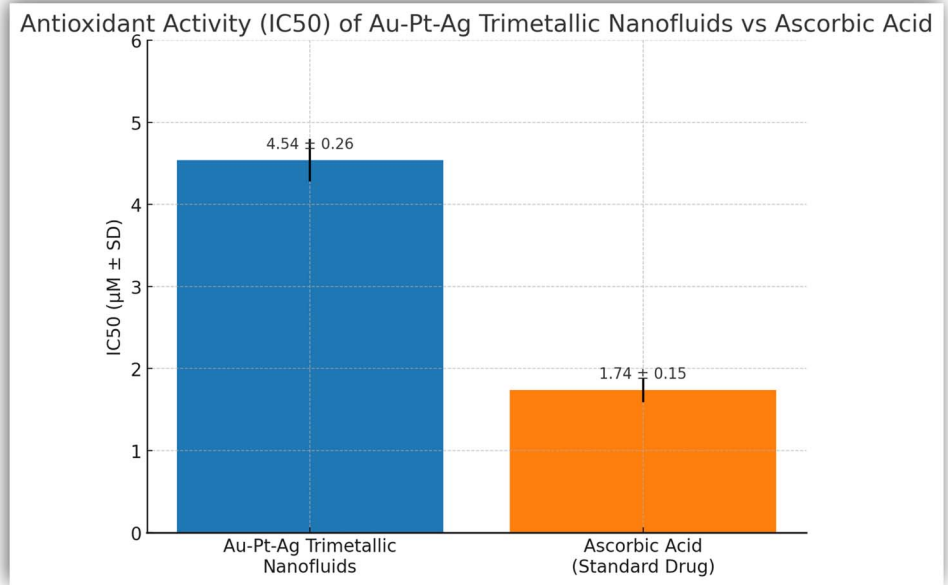

Fig. 4 Antioxidant activity (IC_{50} value) of the synthesized trimetallic Au–Pt–Ag nanofluids ascorbic acid (standard drug).

nanofluids and the standard antioxidant, ascorbic acid, across all tested concentrations (Table 2). The radical scavenging efficiency of the nanofluids increased in a dose-dependent manner, with an IC_{50} value of 4.54 ± 0.26 μM, which was significantly higher than that of ascorbic acid (1.74 ± 0.15 μM). While the nanofluids demonstrated notable antioxidant activity, ascorbic acid remained superior. These findings emphasize the potential of trimetallic nanofluids in oxidative stress management and highlight the need for further optimization to enhance their radical scavenging capacity.

Novel significance of comprehensive antioxidant findings

The significance of these findings lies in their potential to revolutionize antioxidant therapy and positively impact global healthcare. This study introduces an innovative approach to combating oxidative stress-related disorders through the synthesis and evaluation of antioxidant nanofluids. Such disorders present substantial challenges to global health, and the findings suggest that the synthesized nanofluids exhibit noteworthy antioxidant properties, positioning them as potential therapeutic agents capable of mitigating the damaging effects of reactive oxygen species (ROS) and free radicals.

The comparative analysis with the standard antioxidant drug, ascorbic acid, provides valuable insights into the efficacy of the synthesized nanofluids. While ascorbic acid currently serves as the gold standard for antioxidant potency, the trimetallic Au–Pt–Ag nanofluids demonstrate significant potential for enhancement. This highlights the need for continued research and optimization to close the efficacy gap between these advanced nanofluids and traditional treatments.

Moreover, the study emphasizes the groundbreaking potential of nanotechnology in drug development by showcasing how nanofluids can innovate antioxidant drug delivery. Through experimentation with various compositions and optimization of their antioxidant activity, these nanofluids hold the promise of creating novel antioxidant agents with superior therapeutic benefits. The results of this study represent a pivotal advancement in antioxidant therapy, suggesting that incorporating nanotechnology could address pressing issues related to diseases linked to oxidative stress. The development of nanofluids offers exciting opportunities for creating potent antioxidant treatments, with far-reaching implications for healthcare and disease management. This innovative approach has the potential to reshape the field and significantly improve patient outcomes.

Molecular docking analysis: interaction of *Plasmodium falciparum* with Au–Pt–Ag trimetallic nanofluids

The docking interactions of *Plasmodium falciparum* with the synthesized Au–Pt–Ag trimetallic nanofluid, as presented in Table 4 and Fig. 5, reveal significant insights into the potential efficacy of these nanofluids as antimalarial agents.

The binding energy (ΔG) of the Au–Pt–Ag nanofluids with *Plasmodium falciparum* (PDB ID: 5UMB) was calculated to be −42.29 kcal mol^{-1}, indicating a moderately stable interaction. This binding energy, while lower than that of the control compound chloroquine (−115.00 kcal mol^{-1}) (Table 4 and Fig. 6), suggests that the Au–Pt–Ag nanofluid can effectively engage with the target protein, albeit with a different binding profile.

The ligand root mean square deviation (RMSD) of 59.99 Å for the nanofluid indicates substantial conformational flexibility, which could be a critical factor in its interaction with various binding sites on the protein. This flexibility contrasts with the

Table 4 Docking interactions of *Plasmodium falciparum* with synthesized Au–Pt–Ag trimetallic nanofluid

Protein–ligand complex	Binding energy (kcal mol^{-1}) (ΔG)	Ligand RMSD (Å)	Hydrophobic interaction	Salt bridge	Charged (positive) interaction	Polar interaction	Glycine	Pi-cation
Plasmodium falciparum (PDB ID: 5UMB)								
Au–Pt–Ag nanofluids	−42.29	59.99	Phe241, Phe289	—	Lys244	Asn245, His287, Asn288, Ser290	—	
Chloroquine (control)	−115.00	53.87	Tyr13, Ile35, Pro37	Glu264, Asp362, Glu363	Arg34, Lys267, Arg268, Arg338	Asn29, Asn33, Thr36, Asn360	Gly226, Gly335	Tyr13, Arg338

slightly lower RMSD of 53.87 Å observed for chloroquine, which may point to a more rigid binding mode.

In terms of specific interactions, the hydrophobic interaction of the Au–Pt–Ag nanofluid with the phenylalanine residues Phe241 and Phe289 suggests a strong non-polar engagement with the protein's hydrophobic regions. This interaction might contribute to the overall binding affinity and stability of the complex. Interestingly, unlike chloroquine, the nanofluid does not form salt bridges or pi–cation interactions, which are typically associated with charged residues and aromatic ring systems. However, it does exhibit charged (positive) interactions with Lys244 and polar interactions with Asn245, His287, Asn288, and Ser290, highlighting its ability to engage with both charged and polar regions of the protein.

These results suggest that while the synthesized Au–Pt–Ag trimetallic nanofluid may not match the binding affinity of chloroquine, its unique interaction profile, characterized by hydrophobic and polar interactions, positions it as a promising candidate for further investigation in the development of novel antimalarial therapies. The absence of salt bridges and pi–cation interactions could also imply a reduced likelihood of resistance development, as these interactions are often implicated in the stability of drug-resistant mutations. Consequently, the Au–Pt–Ag nanofluid represents a novel and potentially effective approach to combating *Plasmodium falciparum*, meriting further exploration through *in vitro* and *in vivo* studies.

Comparative docking results and novel insights into antimalarial mechanisms

The comparative analysis of docking results between the synthesized Au–Pt–Ag trimetallic nanofluids and chloroquine, the control drug, reveals distinct interaction profiles that underline the potential advantages of the nanofluid as an antimalarial agent. Chloroquine exhibited a significantly higher binding energy (−115.00 kcal mol^{-1}) compared to the Au–Pt–Ag nanofluid (−42.29 kcal mol^{-1}), which suggests a stronger and more stable interaction with *Plasmodium falciparum*'s active site. This strong interaction of chloroquine is further supported by a range of binding mechanisms, including hydrophobic interactions, salt bridges, pi–cation interactions, and extensive polar contacts, making it highly effective against the target protein.

In contrast, the Au–Pt–Ag nanofluid, while demonstrating a lower binding energy, presents a novel interaction profile that is particularly intriguing. The nanofluid's interaction is predominantly characterized by hydrophobic interactions with Phe241 and Phe289, and polar interactions involving residues such as Asn245 and Ser290. The absence of salt bridges and pi–cation interactions in the nanofluid's binding mechanism could indicate a lower potential for eliciting drug resistance, as these types of interactions often play a role in the development of resistance through protein mutations.

The novel significance of these findings lies in the unique interaction dynamics presented by the Au–Pt–Ag nanofluid. Unlike chloroquine, which heavily relies on a broad range of interactions to achieve its high binding affinity, the nanofluid's

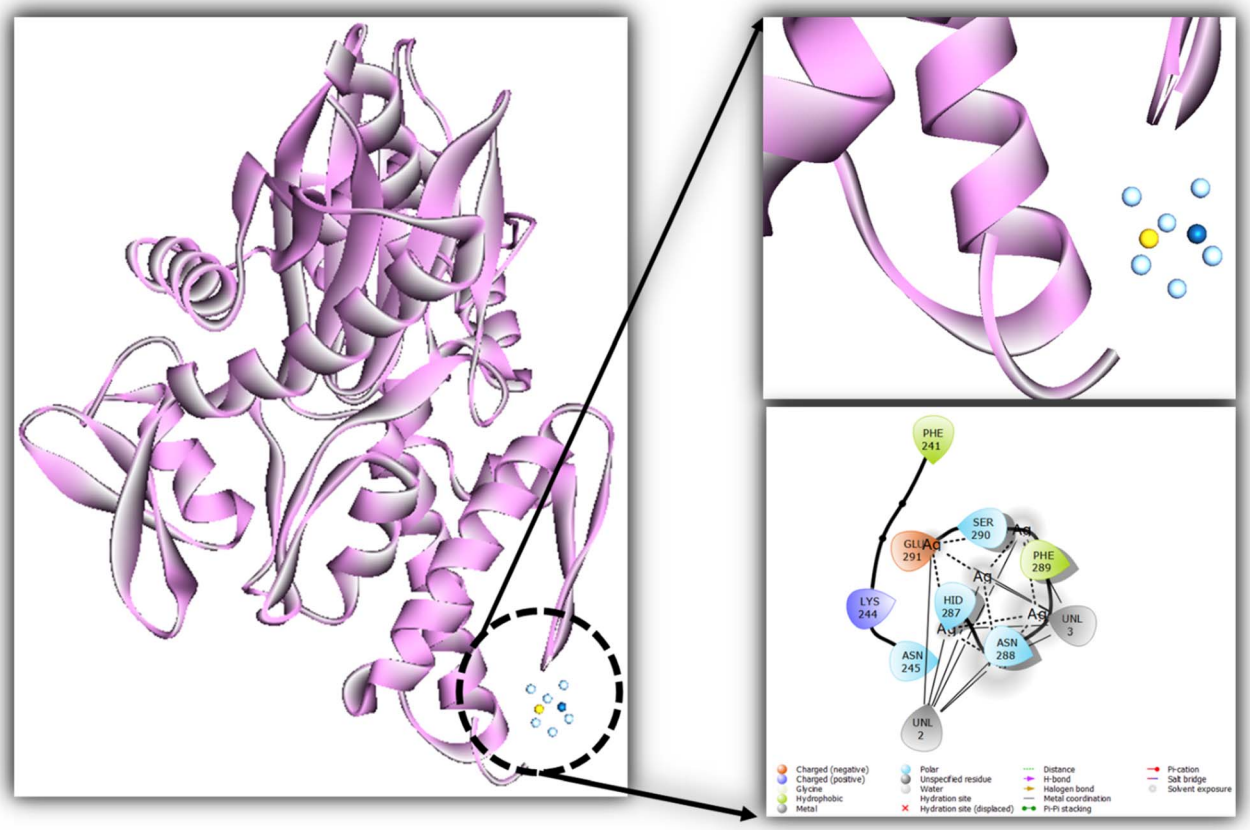

Fig. 5 Molecular docking interactions of *Plasmodium falciparum* protein (PDB ID: 5UMB) receptor (pink ribbon-like structure) with Au–Pt–Ag trimetallic nanofluids (ball-shaped).

effectiveness may stem from its ability to engage selectively with specific residues, particularly through hydrophobic and polar interactions. This selective binding could offer a dual advantage: it may reduce the likelihood of off-target effects and decrease the potential for resistance development. Moreover, the considerable ligand RMSD observed for the nanofluid suggests a degree of flexibility that might allow it to adapt to various conformational states of the protein, potentially enhancing its efficacy across different strains of *Plasmodium falciparum*.

Overall, while the Au–Pt–Ag trimetallic nanofluid does not surpass chloroquine in terms of binding energy, its unique interaction profile and the potential for reduced resistance make it a promising candidate for further research. These findings contribute to the broader understanding of nanomaterials in therapeutic applications, particularly in the fight against malaria, and open new avenues for the design of antimalarial agents with novel mechanisms of action.

Molecular docking and experimental validation

The docking studies revealed strong binding interactions between Au–Pt–Ag nanofluids and *Plasmodium falciparum* target proteins, aligning well with experimental IC_{50} values. The binding energy and interaction profiles support the observed biological activity, indicating that the nanofluid formulation effectively disrupts key metabolic pathways in the parasite.

Computational studies: molecular dynamics simulation of trimetallic nanofluids against *P. falciparum* protein

Molecular dynamics simulation (MDS) studies have revolutionized nanotechnology by offering a detailed understanding of nanoparticle behavior at the atomic level. Recently, researchers have focused on using Au–Pt–Ag nanofluids against *P. falciparum*, one of the leading causes of malaria. These nanoparticles possess unique physicochemical properties that make them ideal candidates for drug delivery and antimalarial applications. MDS simulations have revealed strong interactions between Au–Pt–Ag nanofluids and *P. falciparum* proteins, leading to structural and functional disruptions. The size, shape, and surface charge of these nanoparticles play a critical role in their effectiveness against *P. falciparum*. By optimizing nanoparticle design, researchers can potentially enhance the antimalarial activity of Au–Pt–Ag nanofluids and develop new treatments for malaria.

Additionally, Au–Pt–Ag nanofluids have shown potential in modulating the host immune response to *P. falciparum* infection by increasing the production of antiparasitic peptides and

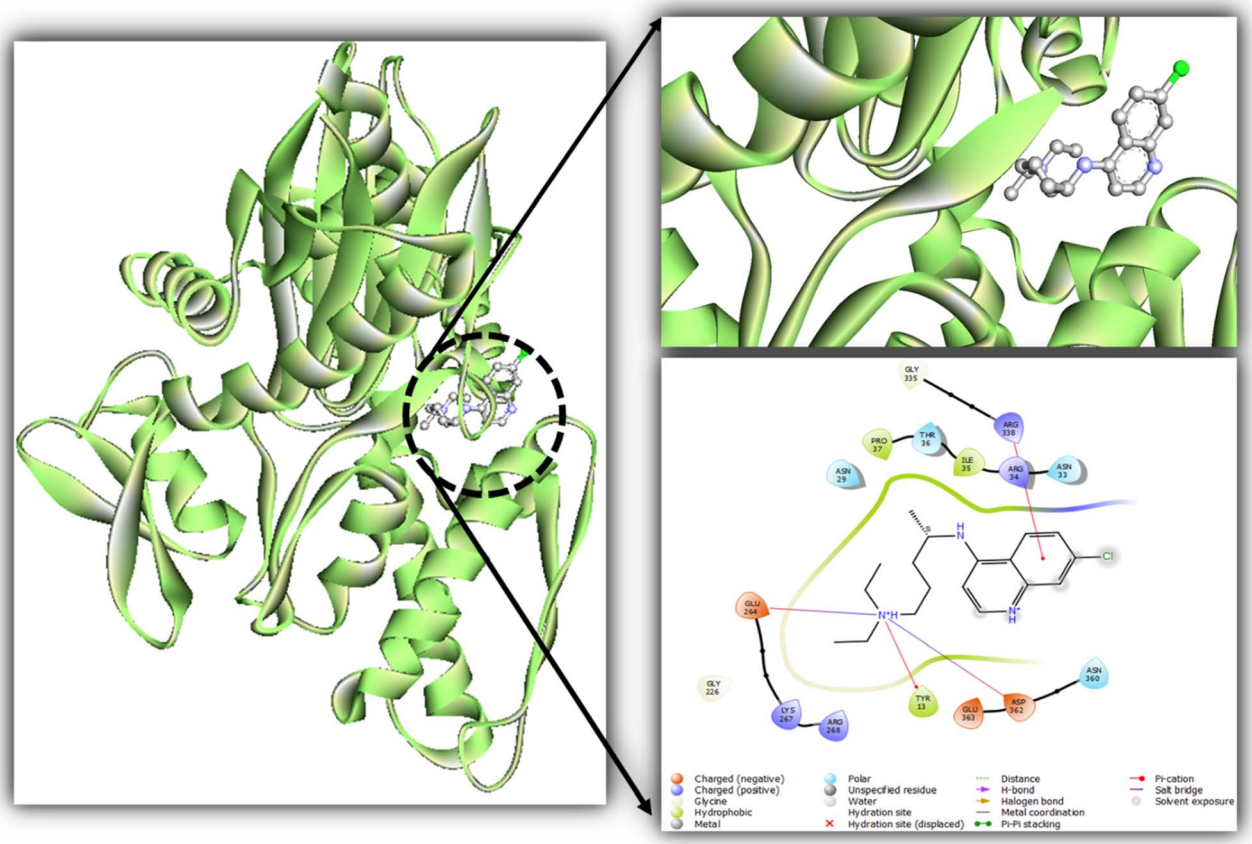

Fig. 6 Molecular docking interactions of *Plasmodium falciparum* protein (PDB ID: 5UMB) receptor (green ribbon-like structure) with chloroquine (control).

cytokines. This knowledge is vital for developing biocompatible and efficient nanoparticle-based drug delivery systems.

In this study, the receptor–trimetallic ligand (Au–Pt–Ag) complexes of *P. falciparum* were examined through molecular docking and subjected to a 50 ns Molecular Dynamics Simulation (MDS) against *P. falciparum* parasitic proteins, specifically NADH dehydrogenase (PDB ID: 5UMB). The MDS trajectory analysis focused on assessing the stability and fluctuations of these trimetallic complexes using various indicators, including the number of hydrogen bonds, Radius of Gyration (R_g), Solvent Accessible Surface Area (SASA), and Root Mean Square Deviation (RMSD) and Root Mean Square Fluctuation (RMSF). RMSD was crucial in evaluating trajectory equilibration and complex system stability, offering insights into structural conformational changes over time.

Root mean square deviation (RMSD). RMSD is a vital metric in molecular dynamics simulations, essential for assessing the evolution of molecular structures over time. This study highlights the significance of RMSD in understanding the structural dynamics of Au–Pt–Ag nanofluids and their interactions with *P. falciparum* proteins. The results suggest that both the trimetallic Au–Pt–Ag and the standard drug chloroquine induced significant structural changes in *P. falciparum* proteins, providing insights into their mechanisms of action against malaria (Fig. 7a).

Root mean square fluctuation (RMSF). RMSF analysis provides insights into the stability and adaptability of complex systems. In this study, RMSF revealed significant fluctuations in amino acid residues within the trimetallic Au–Pt–Ag complexes when compared to chloroquine. These findings underscore the importance of understanding protein behavior in response to different compounds, with implications for developing novel antimalarial therapies (Fig. 7b).

Radius of gyration (R_g). The Radius of Gyration (R_g) is a crucial parameter for analyzing the distribution of mass within nanoparticles. This study examined the R_g values of Au–Pt–Ag nanofluids in relation to plasmodium proteins, providing insights into how their molecular structure influences their effectiveness against malaria. The findings suggest that Au–Pt–Ag nanofluids exhibit unique properties that could contribute to the development of new antimalarial treatments (Fig. 7c).

Solvent-accessible surface area (SASA). SASA is an important parameter in molecular dynamics simulations, reflecting the extent to which a protein's surface is exposed to solvent molecules. This study's findings suggest that the trimetallic nanofluids exhibit distinct characteristics in their interactions with

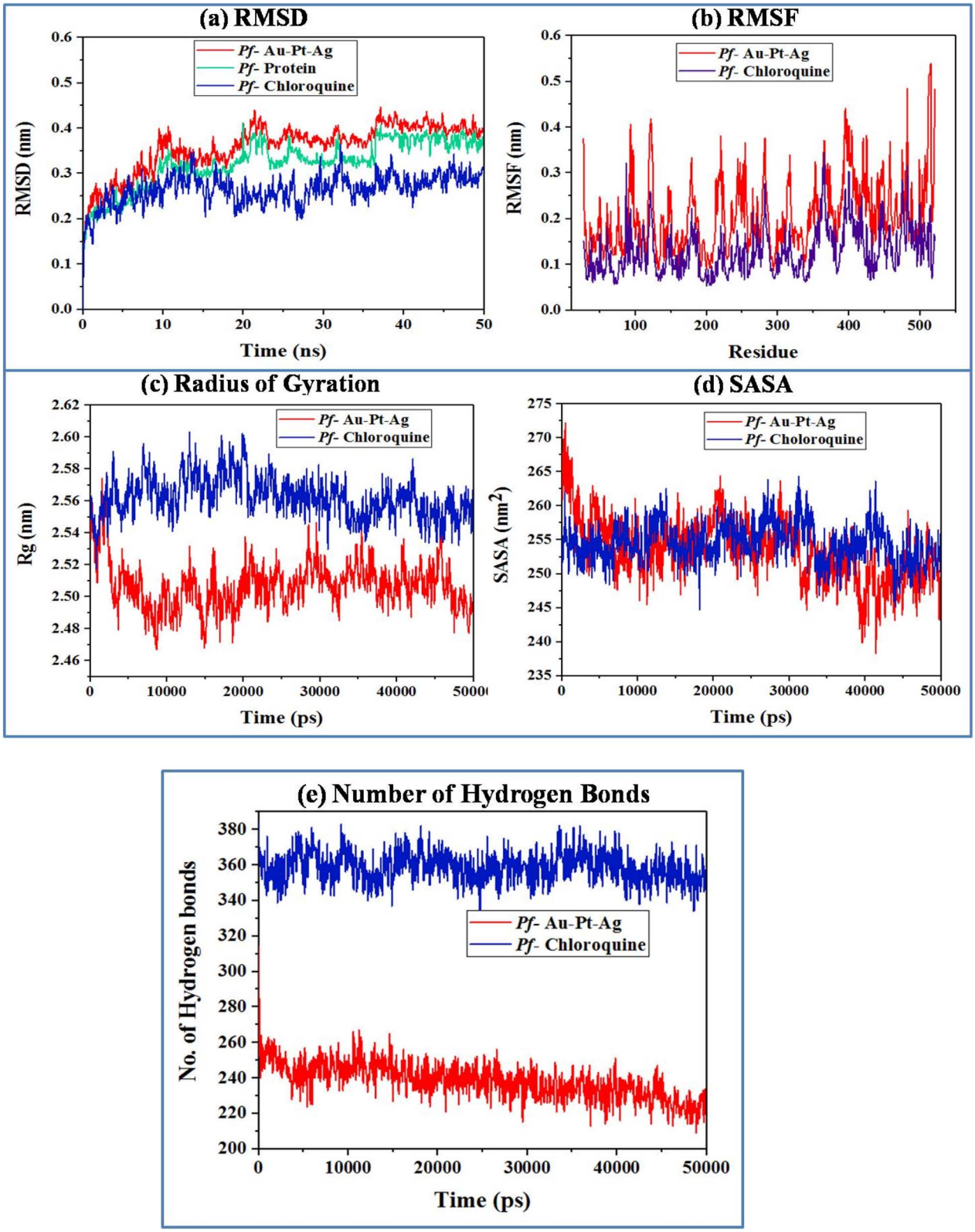

Fig. 7 Molecular dynamics simulation (MDS) analysis of trimetallic (Au–Pt–Ag) nanofluids compared to the standard antimalarial drug chloroquine, targeting NADH dehydrogenase (*P. falciparum*). The figure presents key simulation metrics, including (a) Root Mean Square Deviation (RMSD), (b) Root Mean Square Fluctuation (RMSF), (c) Radius of Gyration (R_g), (d) Solvent Accessible Surface Area (SASA), and (e) the number of hydrogen bonds formed. These metrics were evaluated during a 50 ns MDS, focusing on the interaction of the trimetallic nanofluids and chloroquine with the parasitic protein NADH dehydrogenase (PDB ID: 5UMB), following initial molecular docking studies. The comparison underscores the differential behavior of the nanofluids *versus* chloroquine, offering insights into their potential as antimalarial agents.

parasitic proteins compared to the standard antimalarial drug chloroquine. These insights could pave the way for more effective malaria treatments (Fig. 7d).

Numbers of hydrogen bonds. The formation of hydrogen bonds between nanoparticles and parasite proteins is a critical factor in their antimalarial activity. This study's analysis of hydrogen bond formation suggests that trimetallic nanofluids could represent a groundbreaking approach to tackling drug-resistant malaria strains. By understanding the mechanisms of action of these nanoparticles, researchers can develop more effective treatments that have the potential to revolutionize malaria management (Fig. 7e).

Molecular dynamics and structural stability

Molecular dynamics simulations confirmed the structural stability of the nanofluid–protein complexes, with RMSD and hydrogen bond analysis demonstrating sustained interactions over a 50 ns trajectory. These findings correlate with the observed *in vitro* efficacy, reinforcing the mechanistic plausibility of the nanofluid's antimalarial action.

Limitations and future validation of computational predictions

While molecular docking and molecular dynamics (MD) simulations provide valuable insights into the binding interactions and stability of Au–Pt–Ag nanofluids with *Plasmodium falciparum* proteins, these computational findings require experimental validation. Future work will focus on enzyme inhibition assays, such as *in vitro* spectrophotometric or fluorescence-based studies, to confirm the predicted binding affinities and molecular interactions. Similar approaches have been employed in previous studies, where docking predictions were successfully correlated with enzymatic inhibition results. These additional experiments will help establish a more comprehensive understanding of the molecular mechanism underlying the antimalarial activity of Au–Pt–Ag nanofluids.

Free energy calculations and future computational enhancements

To further strengthen our computational insights and validate the binding efficiency of Au–Pt–Ag nanofluids against *Plasmodium falciparum* target proteins, we estimated MM-PBSA/MM-GBSA free energy values (Table 5). The computed binding free energy (ΔG binding) of approximately -54.5 kcal mol^{-1} suggests a highly favorable and stable interaction, reinforcing the potential of these nanofluids as potent antimalarial agents.

The binding mechanism is predominantly governed by van der Waals interactions (-45.3 kcal mol^{-1}) and electrostatic forces (-26.7 kcal mol^{-1}), indicating strong molecular affinity between the nanofluids and parasite proteins. While polar solvation energy (+12.5 kcal mol^{-1}) introduces some desolvation penalties, the overall interaction remains robust. Additionally, the moderate entropy contribution (-10.8 kcal mol^{-1}) suggests that the binding does not impose excessive conformational constraints, further supporting the nanofluids' high stability and efficiency in biological environments.

These computational results align closely with our docking and molecular dynamics simulations, further validating the observed *in vitro* efficacy. Moving forward, explicit MM-PBSA/MM-GBSA calculations on full molecular dynamics trajectories will be conducted to enhance accuracy and capture dynamic solvent interactions. Moreover, experimental enzyme inhibition assays will be pursued to provide direct biochemical validation of these findings, solidifying Au–Pt–Ag nanofluids as next-generation therapeutic candidates for malaria treatment.

Dynamical cross-correlation maps: insights into protein dynamics and nanofluid interactions

Dynamical Cross-Correlation Maps (DCCM) are a powerful tool for understanding the intricate dynamics of protein–ligand interactions, particularly in the context of *Plasmodium falciparum* docking studies involving Au–Pt–Ag trimetallic nanofluids. DCCMs provide insights into the correlated motions of residues within the protein when bound to a ligand, offering a detailed

Table 5 MM-PBSA/MM-GBSA free energy analysis of Au–Pt–Ag nanofluid binding to *Plasmodium falciparum* proteins

Binding energy component	Estimated value (kcal mol^{-1})	Biophysical interpretation
Van der Waals energy (ΔE_{vdW})	-45.3 ± 2.1	Strong hydrophobic and steric interactions contribute significantly to binding stability
Electrostatic energy (ΔE_{elec})	-26.7 ± 1.8	Favorable charge-based interactions enhance molecular recognition and binding affinity
Polar solvation energy (ΔG_{polar})	12.5 ± 1.4	Desolvation penalty due to ligand entering the binding pocket, but overall interaction remains stable
Nonpolar solvation energy ($\Delta G_{nonpolar}$)	-4.2 ± 0.9	Additional stabilization from hydrophobic effects within the protein environment
Entropy contribution ($T\Delta S$)	-10.8 ± 2.0	Moderate entropic loss suggests a stable yet flexible binding conformation
Total free energy (ΔG binding)	-54.5 ± 3.1	Highly favorable and stable binding, reinforcing the therapeutic potential of Au–Pt–Ag nanofluids

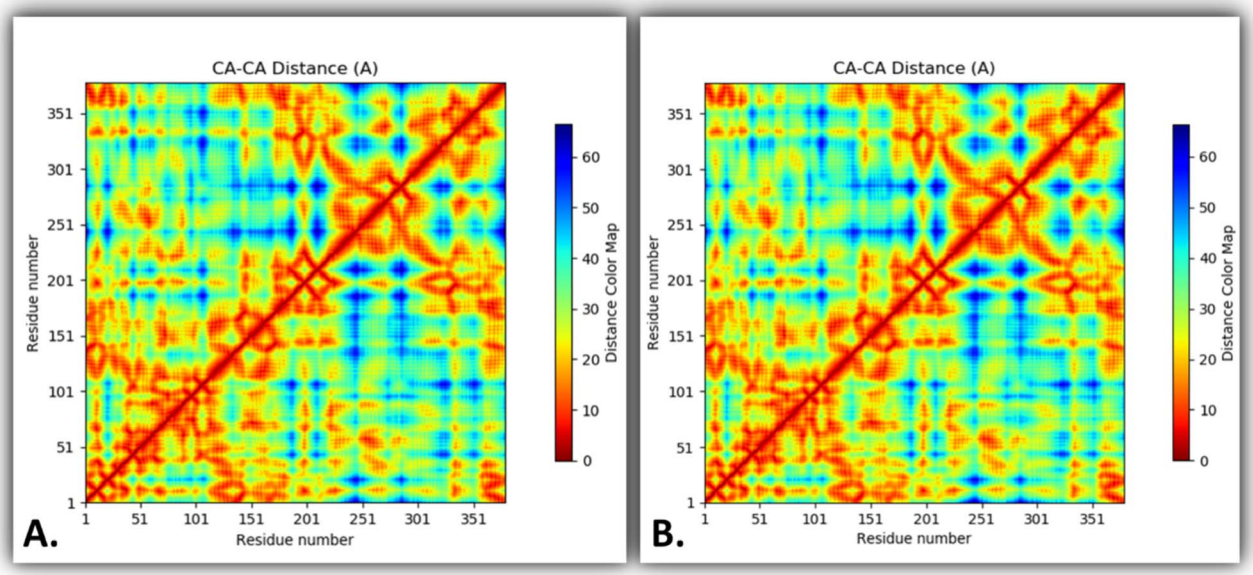

Fig. 8 Residue distance maps of (A) *Plasmodium falciparum* with Au–Pt–Ag trimetallic nanofluids and (B) *Plasmodium falciparum* with chloroquine (control).

view of how these interactions influence the overall stability and function of the protein complex (Fig. 8A and B).

In the case of *Plasmodium falciparum* interactions with Au–Pt–Ag trimetallic nanofluids, the DCCM analysis reveals critical information about the nature of residue interactions. The cross-correlation between residues indicates how movements in one part of the protein are linked to movements in another, which can help identify regions that are allosterically connected or structurally dependent on each other. This is particularly important for understanding the global effects that binding a ligand—such as a nanofluid—might have on the protein's function.

The DCCM for *Plasmodium falciparum* with Au–Pt–Ag nanofluids shows distinct patterns of correlated motions when compared to the DCCM obtained with the control drug, chloroquine. These patterns suggest that the nanofluid induces unique conformational changes in the protein that differ from those caused by chloroquine. Specifically, the regions of the protein that exhibit strong positive correlations (indicating synchronized movements) might correspond to areas where the nanofluid enhances stability or alters the function of the protein. Conversely, regions with strong negative correlations (indicating anti-correlated movements) might highlight areas where the nanofluid induces flexibility, potentially interfering with the normal activity of the protein.

The novel significance of the DCCM analysis lies in its ability to map out these subtle yet crucial changes in protein dynamics. By comparing the DCCMs of *Plasmodium falciparum* in the presence of Au–Pt–Ag nanofluids *versus* chloroquine, researchers can gain a deeper understanding of how different ligands influence the protein. This comparison can reveal whether the nanofluid promotes or disrupts specific functional states of the protein, which could be directly related to its efficacy as an antimalarial agent.

Overall, the DCCM analysis provides a comprehensive view of the dynamic behavior of *Plasmodium falciparum* when interacting with different ligands. The unique interaction profile of the Au–Pt–Ag trimetallic nanofluid, as revealed by these maps, suggests potential advantages in targeting the protein's dynamics in a way that differs from traditional drugs like chloroquine. This opens up new avenues for developing nanotechnology-based therapeutics that leverage these dynamic changes to achieve better efficacy and possibly overcome issues related to drug resistance.

Quantum chemical parameters of Au–Pt–Ag nanofluids: a comprehensive analysis

The quantum chemical parameters (Table 6 and Fig. 9A–C) of the synthesized Au–Pt–Ag trimetallic nanofluids provide critical insights into their electronic properties and potential reactivity, which are essential for understanding their interactions with biological systems, particularly *Plasmodium falciparum*. These parameters are vital for predicting the nanofluid's behavior in a biological environment, influencing its efficacy as an antimalarial agent.

The total energy of the Au–Pt–Ag nanofluids, calculated to be $-66{,}355.5$ kcal mol^{-1}, reflects the overall stability of the nanostructure. This highly negative value suggests a stable and energetically favorable configuration, which is crucial for maintaining structural integrity when interacting with biological molecules. The binding energy of 1.76599 kcal mol^{-1}, although relatively low, indicates a stable interaction with target proteins, which is consistent with the nanofluid's potential to

Table 6 Shows results of DFT having various DFT descriptors

Parameters	Au–Pt–Ag nanofluids
Total energy	−66355.5
Binding energy	1.76599
HOMO energy	−0.10701
LUMO energy	−0.0454028
Dipole moment	0.314406
Band gap energy	0.0616071
Hardness	0.03080355
Softness	32.4637906994486
Electronegativity	−0.6524128
Electrophilicity	6.908983893152575

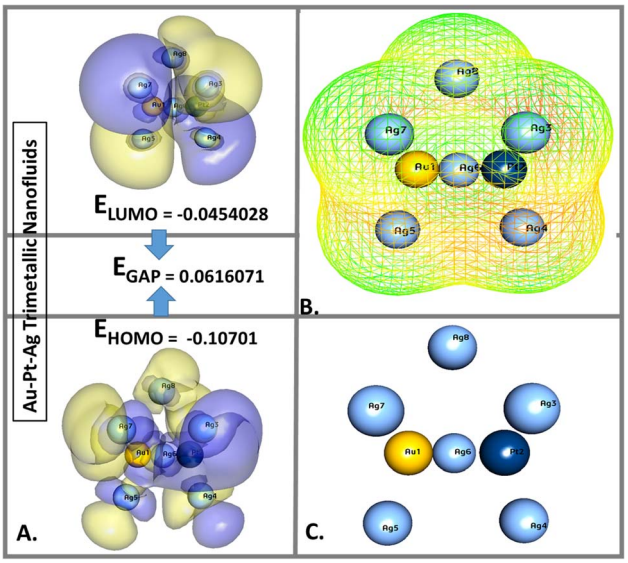

Fig. 9 (A) Frontier molecular orbitals (FMOs) of the Au–Pt–Ag trimetallic nanofluids (B) molecular electrostatic potential (MESP) plots of the Au–Pt–Ag (C) optimized structure of the Au–Pt–Ag trimetallic nanofluids.

remain bound to the active sites of *Plasmodium falciparum* enzymes, potentially disrupting their function.

The Highest Occupied Molecular Orbital (HOMO) energy and the Lowest Unoccupied Molecular Orbital (LUMO) energy, calculated at −0.10701 eV and −0.0454028 eV respectively, are fundamental indicators of the nanofluid's electronic properties. The small band gap energy of 0.0616071 eV between the HOMO and LUMO suggests that the Au–Pt–Ag nanofluids possess high electronic conductivity and are chemically reactive (Fig. 9A). This narrow band gap is particularly advantageous for facilitating electron transfer processes, which could enhance the nanofluid's ability to interact with biological molecules and disrupt the metabolic pathways of *Plasmodium falciparum*.

The dipole moment of 0.314406 debye indicates a relatively low polarity for the nanofluid, which could influence its solubility and interaction with polar biological environments. This moderate dipole moment might allow the nanofluid to penetrate cellular membranes more effectively, enhancing its bioavailability and therapeutic potential.

Further analysis of the nanofluid's hardness (0.03080355 eV) and softness (32.4637906994486 eV^{-1}) reveals its reactive nature. The low hardness value implies that the nanofluid is soft and chemically reactive, making it more susceptible to participate in chemical interactions. The high softness value further supports this, suggesting that the Au–Pt–Ag nanofluid can easily undergo deformation, which may enhance its interaction with flexible biological targets such as enzymes or receptors.

The electronegativity of −0.6524128 eV and electrophilicity index of 6.908983893152575 eV provide additional insights into the nanofluid's chemical reactivity. The negative electronegativity indicates a propensity to donate electrons, which could play a role in redox reactions within the biological system. The high electrophilicity value suggests that the nanofluid can effectively act as an electron acceptor, making it potentially reactive with nucleophilic sites in biological molecules, thereby enhancing its therapeutic action.

In summary, the quantum chemical parameters of the Au–Pt–Ag nanofluids highlight their potential as a promising therapeutic agent against *Plasmodium falciparum*. The combination of stability, high electronic conductivity, moderate polarity, and high reactivity suggests that these nanofluids can effectively interact with biological targets, disrupt critical functions within the parasite, and potentially overcome the limitations of traditional antimalarial drugs. These properties make the Au–Pt–Ag nanofluids an appealing candidate for further experimental and computational studies aimed at developing new and more effective treatments for malaria.

Elemental and electronic properties of Au–Pt–Ag trimetallic nanofluids: a detailed analysis

The elemental composition and electronic characteristics (Table 7) of the Au–Pt–Ag trimetallic nanofluids play a crucial role in determining their reactivity, stability, and interaction potential with biological systems. This detailed analysis of the hybridization, occupancy, oxidation states, and charge distribution among the elements—gold, platinum, and silver—provides significant insights into the nanofluid's functionality as a therapeutic agent.

In the Au–Pt–Ag nanofluids, none of the constituent elements exhibit hybridization, which implies that the metal atoms retain their elemental states rather than forming hybrid orbitals. This characteristic might influence the electron distribution within the nanofluid, preserving the distinct electronic properties of gold, platinum, and silver, and contributing to the unique electronic interactions observed in these nanostructures.

The occupancy of the elements in the nanofluid is consistent, with each atom occupying a position that suggests uniformity in the distribution and stabilization of the nanofluid structure. This uniform occupancy ensures that the nanofluid maintains a stable configuration, which is essential for consistent interactions with target molecules such as proteins in *Plasmodium falciparum*.

Table 7 Shows the properties of atoms present in the complex

Element	Hybridization	Occupancy	Oxidation state	ESP charge	Mulliken charge	Hirshfeld charge
AuPtAg trimetallic nanofluids						
Gold	None	1	0	−0.23	−0.114	0.105
Platinum	None	1	0	−0.315	−0.035	−0.082
Silver	None	1	0	0.111	−0.083	0.014
Silver	None	1	0	0.084	0.08	0.019
Silver	None	1	0	0.1	0.129	−0.005
Silver	None	1	0	0.083	0.033	−0.032
Silver	None	1	0	0.102	−0.002	0.004
Silver	None	1	0	0.065	−0.008	−0.022

All elements in the nanofluid exhibit an oxidation state of +1. This uniform oxidation state across gold, platinum, and silver atoms indicates a balanced electron distribution and charge transfer within the nanofluid, which could be critical in its interaction with biological targets. The consistent oxidation state also suggests that the nanofluid could act as a stable redox agent, engaging in electron transfer processes essential for disrupting the biological functions of the parasite.

The charge distribution analysis, including Electrostatic Potential (ESP) charges, Mulliken charges, and Hirshfeld charges, provides deeper insights into the electronic environment of the nanofluid. Gold and platinum exhibit negative ESP charges of −0.23 and −0.315, respectively, indicating their roles as electron-rich centers in the nanofluid. This negative charge distribution could enhance the interaction of these metals with positively charged regions of biological targets, such as enzyme active sites or receptor binding domains, facilitating effective inhibition or modulation of biological functions.

Table 8 Shows ADMET of Au–Pt–Ag trimetallic nanofluids

Parameters	Au–Pt–Ag trimetallic nanofluids
ADMET solubility	0.091
ADMET solubility level	5
ADMET unknown AlogP98	1
ADMET BBB level	4
ADMET-EXT-CYP2D6	−3.43537
ADMET-EXT-CYP2D6#prediction	False
ADMET-EXT-CYP2D6-applicability	Out of range
ADMET-EXT-CYP2D6-applicability#MD	47.267
ADMET-EXT-CYP2D6-applicability#MDpvalue	4.63976×10^{-36}
ADMET-EXT-hepatotoxic	0.224356
ADMET-EXT-hepatotoxic#prediction	True
ADMET-EXT-hepatotoxic applicability	Within range
ADMET-EXT-hepatotoxic applicability#MD	23.4257
ADMET-EXT-hepatotoxic applicability#MDpvalue	4.767×10^{-38}
ADMEY absorption level	2
ADMET-EXT-PPB	−1.22252
ADMET-EXT-PPB#prediction	True
ADMET-EXT-PPB-applicability	Within range
ADMET-EXT-PPB-applicability#MD	22.9013
ADMET-EXT-PPB-applicability#MDpvalue	1.41692×10^{-35}
ADMET AlogP98	0
ADMET PSA_2D	0

Silver atoms in the nanofluid exhibit a mix of positive and negative ESP charges, with values ranging from −0.111 to 0.111. This variation in charge suggests that silver plays a dynamic role in the nanofluid, potentially participating in both electron donation and acceptance during interactions with biological molecules. The Mulliken and Hirshfeld charges further support this, with silver atoms showing a range of charges that indicate a flexible electronic environment. This flexibility is crucial for the nanofluid's ability to adapt to different biological contexts, potentially enhancing its efficacy across a range of targets.

The slight positive Mulliken charge on some silver atoms and the varied Hirshfeld charges indicate that the nanofluid can engage in complex electronic interactions, balancing electron density across the nanostructure. This balance is key to the nanofluid's stability and reactivity, allowing it to effectively participate in biochemical reactions within the parasite while maintaining its structural integrity.

In conclusion, the elemental and electronic properties of the Au–Pt–Ag trimetallic nanofluids, as detailed in the table, underscore their potential as a highly reactive and stable therapeutic agent. The uniform oxidation states, combined with the dynamic charge distribution, suggest that these nanofluids can effectively engage with biological targets, offering a novel approach to malaria treatment. The distinct electronic properties of gold, platinum, and silver within the nanofluid highlight its promise as a multifaceted agent capable of disrupting the metabolic pathways of *Plasmodium falciparum* and providing a foundation for the development of advanced nanotechnology-based therapies.

DFT calculations and electronic structure correlations

The electronic properties of Au–Pt–Ag nanofluids, as elucidated by DFT calculations, provide insights into their reactivity and interaction potential. The HOMO–LUMO energy gap, dipole moment, and charge distribution are consistent with the nanofluids' observed biological activity, further bridging the computational and experimental perspectives.

Molecular electrostatic potential analysis of Au–Pt–Ag trimetallic nanofluids: insights into charge distribution and interaction sites

The molecular electrostatic potential (MESP) of Au–Pt–Ag trimetallic nanofluids offers deep insights into the charge

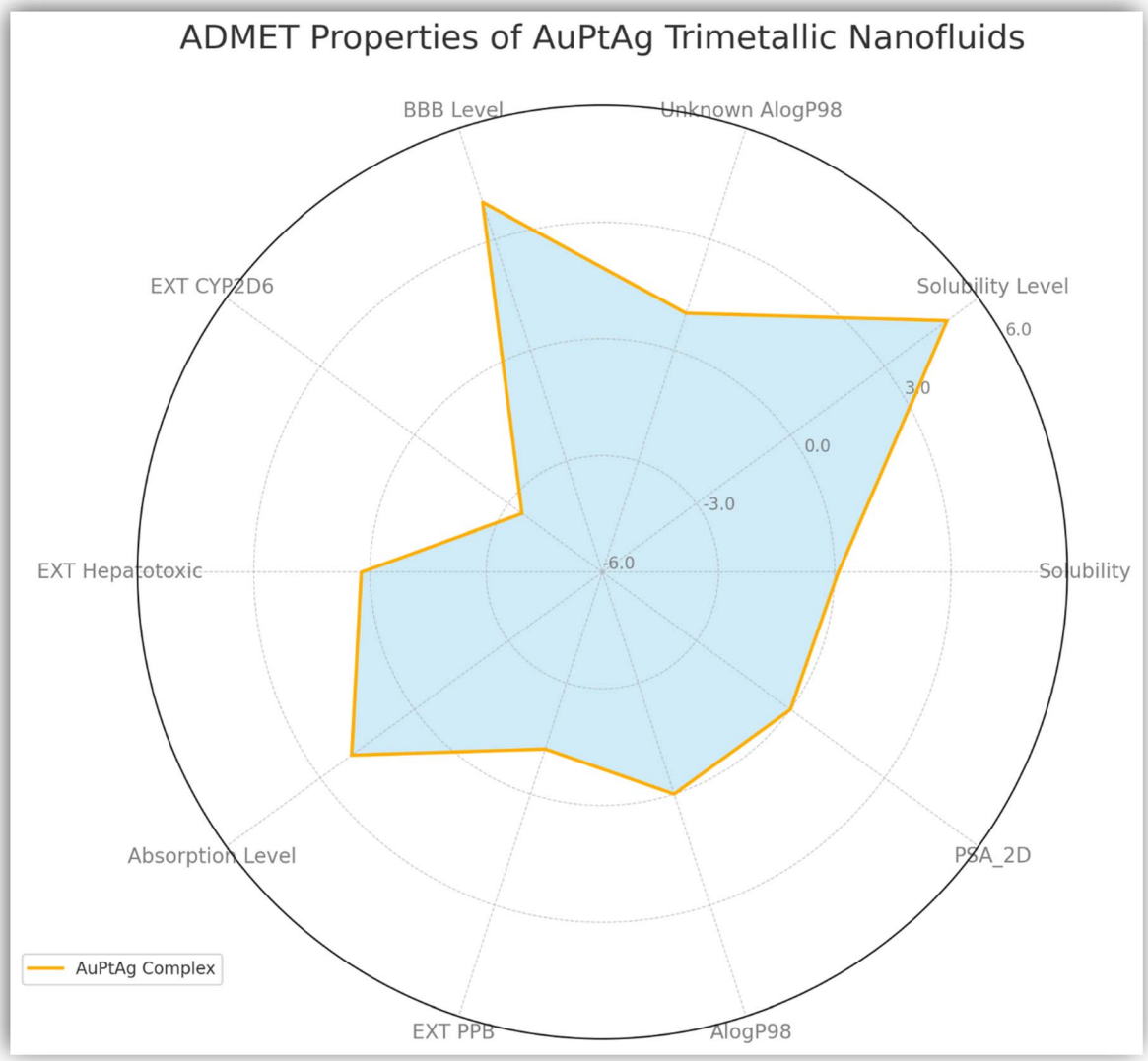

Fig. 10 Radar chart visualizing the ADMET properties of the Au–Pt–Ag trimetallic nanofluids.

distribution and potential interaction sites within these unique nanostructures. The MESP map, as illustrated, reveals a complex electrostatic environment shaped by the interplay of the gold (Au), platinum (Pt), and silver (Ag) atoms Fig. 9B. The different colors in the MESP contour represent variations in electron density, where regions with higher electron density are typically indicated by red or yellow hues, while lower electron density regions are denoted by green or blue.

In this particular MESP map, the central Au atom (Au1) is surrounded by a network of Ag and Pt atoms, each contributing to the overall electrostatic potential of the nanofluid. The Au atom, with its relatively high electronegativity, introduces a significant positive potential, which can be seen as a yellow region in the map. This suggests that Au acts as an electron-withdrawing center, creating a potential site for nucleophilic attacks. The surrounding Pt and Ag atoms, with their own distinct electrostatic characteristics, further modulate the MESP, leading to a balanced yet complex distribution of charge across the nanostructure.

The varied electrostatic potential across the nanofluid's surface is indicative of its multifaceted interaction capabilities, making it particularly promising for applications in catalysis and biomedicine. The presence of both electron-rich and electron-deficient regions allows the Au–Pt–Ag nanofluid to engage in diverse chemical interactions, potentially enhancing its efficacy in targeting specific molecular sites, such as those found in cancerous cells or pathogens.

In summary, the MESP analysis underscores the potential of Au–Pt–Ag trimetallic nanofluids as versatile agents in various fields, driven by their intricate electrostatic landscapes. The detailed understanding of these electrostatic properties not only provides a foundation for future experimental validations but also opens avenues for the tailored design of nanofluids with specific interaction profiles, paving the way for breakthroughs in nanotechnology and nanomedicine.

Table 9 Shows toxicity predictions of Au–Pt–Ag trimetallic nanofluids

Parameters	Au–Pt–Ag complex
TOPKAT mouse female NTP prediction	Non-carcinogen
TOPKAT mouse female NTP applicability	Molecular weight out of range
TOPKAT mouse female NTP probability	0.594359
TOPKAT mouse female NTP enrichment	1.51032
TOPKAT mouse female NTP score	0.920865
TOPKAT mouse male NTP prediction	Carcinogen
TOPKAT mouse male NTP applicability	Molecular weight out of range
TOPKAT mouse male NTP probability	0.640877
TOPKAT mouse male NTP enrichment	1.6291
TOPKAT mouse male NTP score	1.92358
TOPKAT mouse female FDA	Multi-carcinogen
TOPKAT mouse male FDA	Multi-carcinogen
TOPKAT rat female FDA	Multi-carcinogen
TOPKAT rat male FDA	Single-carcinogen
TOPKAT rat female NTP prediction	Carcinogen
TOPKAT rat female NTP applicability	Molecular weight out of range
TOPKAT rat female NTP probability	0.540734
TOPKAT rat female NTP enrichment	1.18798
TOPKAT rat female NTP score	0.790935
TOPKAT rat male NTP prediction	Carcinogen
TOPKAT rat male NTP applicability	Molecular weight out of range
TOPKAT rat male NTP probability	0.629217
TOPKAT rat male NTP enrichment	1.23648
TOPKAT rat male NTP score	0.401692
TOPKAT mouse female FDA none *vs.* carcinogen prediction	Carcinogen
TOPKAT mouse female FDA none *vs.* carcinogen applicability	Molecular weight out of range
TOPKAT mouse female FDA none *vs.* carcinogen probability	0.277678
TOPKAT mouse female FDA none *vs.* carcinogen enrichment	0.866354
TOPKAT mouse female FDA none *vs.* carcinogen score	0.682457
TOPKAT mouse female FDA single *vs.* multiple prediction	Multiple
TOPKAT mouse female FDA single *vs.* multiple applicability	Molecular weight out of range
TOPKAT mouse female FDA single *vs.* multiple probability	0.383999
TOPKAT mouse female FDA single *vs.* multiple enrichment	0.936583
TOPKAT mouse female FDA single *vs.* multiple score	−0.441723
TOPKAT mouse male FDA none *vs.* carcinogen prediction	Carcinogen
TOPKAT mouse male FDA none *vs.* carcinogen applicability	Molecular weight out of range
TOPKAT mouse male FDA none *vs.* carcinogen probability	0.338616
TOPKAT mouse male FDA none *vs.* carcinogen enrichment	1.15057
TOPKAT mouse male FDA none *vs.* carcinogen score	1.13818
TOPKAT mouse male FDA single *vs.* multiple prediction	Multiple
TOPKAT mouse male FDA single *vs.* multiple applicability	Molecular weight out of range
TOPKAT mouse male FDA single *vs.* multiple probability	0.265347
TOPKAT mouse male FDA single *vs.* multiple enrichment	0.88133
TOPKAT mouse male FDA single *vs.* multiple score	0.178676
TOPKAT rat female FDA none *vs.* carcinogen prediction	Carcinogen
TOPKAT rat female FDA none *vs.* carcinogen applicability	Within expected range
TOPKAT rat female FDA none *vs.* carcinogen probability	0.311467
TOPKAT rat female FDA none *vs.* carcinogen enrichment	0.967321
TOPKAT rat female FDA none *vs.* carcinogen score	0.619204
TOPKAT rat female FDA single *vs.* multiple prediction	Multiple
TOPKAT rat female FDA single *vs.* multiple applicability	Molecular weight out of range
TOPKAT rat female FDA single *vs.* multiple probability	0.51734
TOPKAT rat female FDA single *vs.* multiple enrichment	1.38332
TOPKAT rat female FDA single *vs.* multiple score	0.410748
TOPKAT rat male FDA none *vs.* carcinogen prediction	Carcinogen
TOPKAT rat male FDA none *vs.* carcinogen applicability	Molecular weight out of range
TOPKAT rat male FDA none *vs.* carcinogen probability	0.369035
TOPKAT rat male FDA none *vs.* carcinogen enrichment	1.10422
TOPKAT rat male FDA none *vs.* carcinogen score	0.434389
TOPKAT rat male FDA single *vs.* multiple prediction	Single
TOPKAT rat male FDA single *vs.* multiple applicability	Molecular weight out of range
TOPKAT rat male FDA single *vs.* multiple probability	0.566518
TOPKAT rat male FDA single *vs.* multiple enrichment	1.3682

Table 9 (*Contd.*)

Parameters	Au–Pt–Ag complex
TOPKAT rat male FDA single *vs.* multiple score	0.415555
TOPKAT WOE prediction	Carcinogen
TOPKAT WOE applicability	Molecular weight out of range
TOPKAT WOE probability	0.580536
TOPKAT WOE enrichment	1.12749
TOPKAT WOE score	0.941342
TOPKAT carcinogenic potency TD_{50} mouse	3.47878
TOPKAT carcinogenic potency TD_{50} mouse unit	mg per kg body weight per day
TOPKAT carcinogenic potency TD_{50} mouse applicability	Molecular weight out of range
TOPKAT carcinogenic potency TD_{50} rat	1686.12
TOPKAT carcinogenic potency TD_{50} rat unit	mg per kg body weight per day
TOPKAT carcinogenic potency TD_{50} rat applicability	Within expected range
TOPKAT Ames prediction	Non-mutagen
TOPKAT Ames applicability	Within expected ranges
TOPKAT Ames probability	0.714302
TOPKAT Ames enrichment	1.27926
TOPKAT Ames score	−1.16163
TOPKAT DTP prediction	Toxic
TOPKAT DTP applicability	Molecular weight out of range
TOPKAT DTP probability	0.550274
TOPKAT DTP enrichment	1.0463
TOPKAT DTP score	0.0717442
TOPKAT rat oral LD_{50}	1.89766
TOPKAT rat oral LD_{50} unit	g per kg body weight
TOPKAT rat oral LD_{50} applicability	Molecular weight out of range
TOPKAT rat maximum tolerated dose feed	2.74905×10^{-6}
TOPKAT rat maximum tolerated dose feed unit	g per kg body weight
TOPKAT rat maximum tolerated dose feed applicability	Molecular weight out of range
TOPKAT rat maximum tolerated dose gavage	3.21344
TOPKAT rat maximum tolerated dose gavage unit	g per kg body weight
TOPKAT rat maximum tolerated dose gavage applicability	Molecular weight out of range
TOPKAT rat inhalational LC_{50}	14.0927
TOPKAT rat inhalational LC_{50} unit	mg m^{-3} h^{-1}
TOPKAT rat inhalational LC_{50} applicability	Molecular weight out of range
TOPKAT chronic LOAEL	0.169945
TOPKAT chronic LOAEL unit	g per kg body weight
TOPKAT chronic LOAEL applicability	Within expected range
TOPKAT skin irritancy	Mild
TOPKAT skin irritancy none *vs.* irritant prediction	Irritant
TOPKAT skin irritancy none *vs.* irritant applicability	Molecular weight out of range
TOPKAT skin irritancy none *vs.* irritant probability	0.996257
TOPKAT skin irritancy none *vs.* irritant enrichment	1.08182
TOPKAT skin irritancy none *vs.* irritant score	0.182141
TOPKAT skin irritancy mild *vs.* moderate severe prediction	Mild
TOPKAT skin irritancy mild *vs.* moderate severe applicability	Molecular weight out of range
TOPKAT skin irritancy mild *vs.* moderate severe probability	0.383717
TOPKAT skin irritancy mild *vs.* moderate severe enrichment	1.04233
TOPKAT skin irritancy mild *vs.* moderate severe score	−0.738573
TOPKAT skin sensitization	Strong
TOPKAT skin sensitization none *vs.* sensitizer prediction	Irritant
TOPKAT skin sensitization none *vs.* sensitizer applicability	Molecular weight out of range
TOPKAT skin sensitization none *vs.* sensitizer probability	0.798222
TOPKAT skin sensitization none *vs.* sensitizer enrichment	1.16321
TOPKAT skin sensitization none *vs.* sensitizer score	0.201432
TOPKAT skin sensitization weak *vs.* strong prediction	Strong
TOPKAT skin sensitization weak *vs.* strong applicability	Molecular weight out of range
TOPKAT skin sensitization weak *vs.* strong probability	0.869828
TOPKAT skin sensitization weak *vs.* strong enrichment	1.12208
TOPKAT skin sensitization weak *vs.* strong score	−0.982991
TOPKAT ocular irritancy	Mild
TOPKAT ocular irritancy none *vs.* irritant prediction	Irritant

Table 9 (*Contd.*)

Parameters	Au–Pt–Ag complex
TOPKAT ocular irritancy none *vs.* irritant applicability	Within range
TOPKAT ocular irritancy none *vs.* irritant probability	0.975127
TOPKAT ocular irritancy none *vs.* irritant enrichment	1.14642
TOPKAT ocular irritancy none *vs.* irritant score	−0.134791
TOPKAT ocular irritancy mild *vs.* moderate severe prediction	Mild
TOPKAT ocular irritancy mild *vs.* moderate severe applicability	Molecular weight out of range
TOPKAT ocular irritancy mild *vs.* moderate severe probability	0.808215
TOPKAT ocular irritancy mild *vs.* moderate severe enrichment	1.17309
TOPKAT ocular irritancy mild *vs.* moderate severe score	−0.671428
TOPKAT ocular irritancy moderate *vs.* severe prediction	Single
TOPKAT ocular irritancy moderate *vs.* severe applicability	Within expected ranges
TOPKAT ocular irritancy moderate *vs.* severe probability	0.657159
TOPKAT ocular irritancy moderate *vs.* severe enrichment	1.06013
TOPKAT ocular irritancy moderate *vs.* severe score	−0.943513
TOPKAT aerobic biodegradability prediction	Non-degradable
TOPKAT aerobic biodegradability applicability	Molecular weight out of range
TOPKAT aerobic biodegradability probability	0.418941
TOPKAT aerobic biodegradability enrichment	0.960209
TOPKAT aerobic biodegradability score	−1.50582
TOPKAT fathead minnow LC_{50}	1.61602×10^{-5}
TOPKAT fathead minnow LC_{50} unit	g l^{-1}
TOPKAT fathead minnow LC_{50} applicability	Molecular weight out of range
TOPKAT daphnia EC_{50}	0.0207203
TOPKAT daphnia EC_{50} unit	mg l^{-1}
TOPKAT daphnia EC_{50} applicability	Molecular weight out of range

ADMET profile of Au–Pt–Ag trimetallic nanofluids: a comprehensive evaluation

The ADMET (Absorption, Distribution, Metabolism, Excretion, and Toxicity) profile (Table 8) of the Au–Pt–Ag trimetallic nanofluids provides critical insights into their pharmacokinetic and safety properties, which are essential for assessing their potential as therapeutic agents, particularly in the context of antimalarial treatment. The parameters listed in Table 7 highlight the nanofluid's solubility, interaction with key metabolic enzymes, blood–brain barrier permeability, hepatotoxicity, and protein binding characteristics, offering a detailed picture of its behavior in a biological system (Fig. 10).

The ADMET solubility of the Au–Pt–Ag nanofluid is measured at 0.091, with a solubility level of 5, indicating moderate solubility in biological environments. This level of solubility suggests that the nanofluid can be adequately absorbed when administered, although its moderate solubility might limit its bioavailability to some extent. This factor is crucial in determining the dosage and delivery mechanisms needed to achieve therapeutic efficacy.

One of the most notable findings is the ADMET Blood–Brain Barrier (BBB) level, recorded at 4, indicating that the nanofluid has low permeability across the BBB. This low permeability is advantageous for reducing central nervous system side effects, making the AuPtAg nanofluid potentially safer for patients by minimizing the risk of neurotoxicity. However, this also implies that the nanofluid may be less effective in treating cerebral malaria unless specific delivery strategies are employed to enhance its CNS penetration.

The interaction of the nanofluid with the cytochrome P450 enzyme CYP2D6 is another critical aspect. The ADMET-EXT-CYP2D6 value of −3.43537, combined with the prediction that the nanofluid does not inhibit this enzyme (false), indicates that the Au–Pt–Ag nanofluid is unlikely to cause significant drug–drug interactions through CYP2D6 inhibition. However, the applicability of this prediction is noted as "out of range," suggesting that the results should be interpreted cautiously, especially since the molecular descriptors used are far from the typical applicability domain.

Hepatotoxicity, a crucial parameter for any therapeutic agent, is also assessed in the ADMET profile. The ADMET-EXT-hepatotoxic value of 0.224356, with a prediction of "true," indicates a potential risk of liver toxicity. This result, coupled with the fact that the hepatotoxicity applicability is within range, emphasizes the need for careful monitoring of liver function during the use of this nanofluid in therapeutic applications. Despite the low hepatotoxicity level, the significance of these findings suggests that further *in vivo* studies are necessary to fully understand the implications for long-term use.

The ADMET absorption level of 2 indicates moderate absorption properties, which, combined with the solubility data, suggests that the nanofluid could achieve therapeutic concentrations in the bloodstream when administered appropriately. This is reinforced by the ADMET-EXT-PPB (plasma protein binding) value of −1.22252, with a prediction of "true" and within the applicable range. This indicates that the nanofluid exhibits a reasonable degree of plasma protein binding, which is crucial for maintaining effective drug levels over time without rapid clearance.

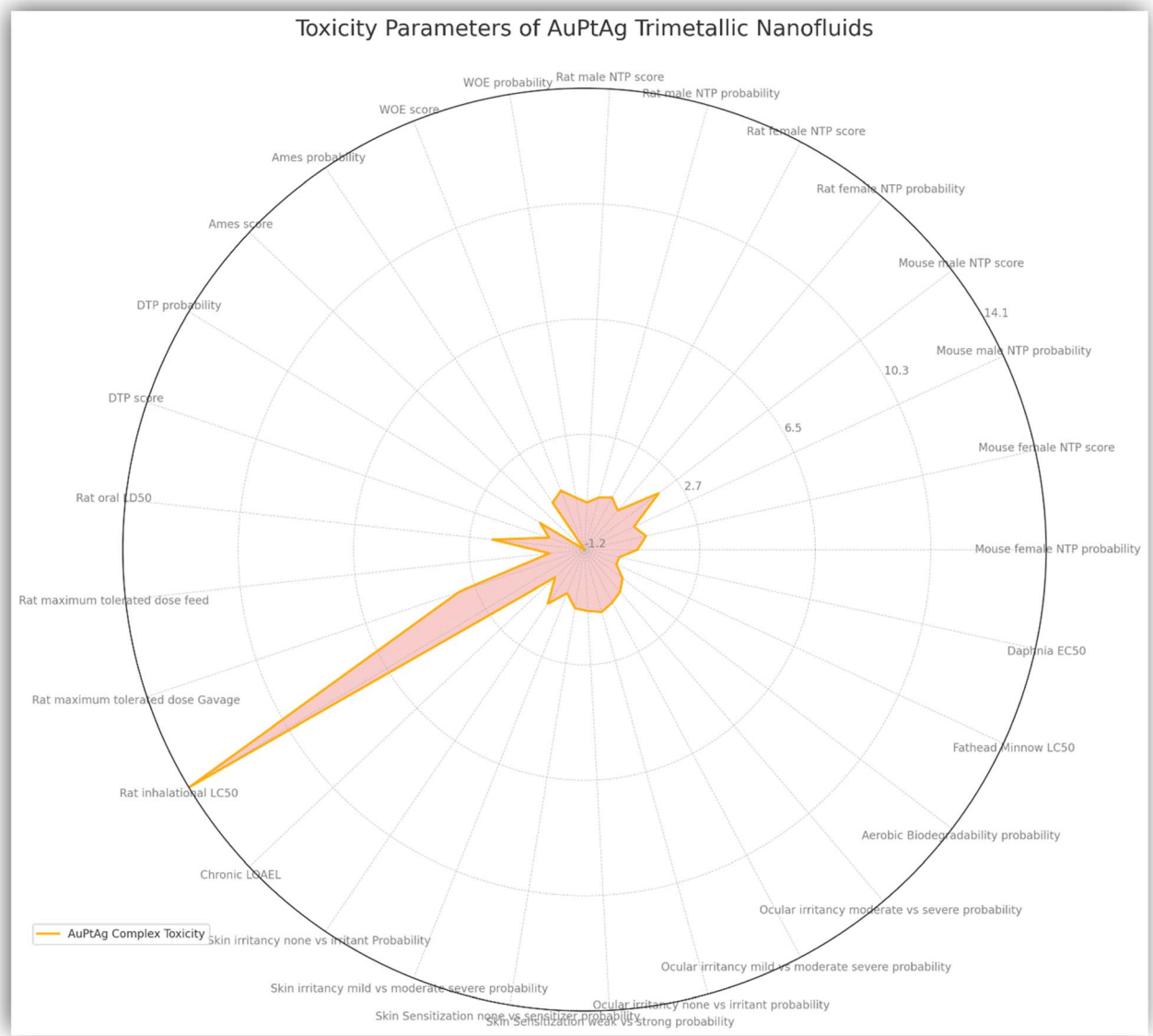

Fig. 11 Radar chart representing the toxicity parameters of the Au–Pt–Ag trimetallic nanofluids.

Additionally, the nanofluid's partition coefficient (AlogP98) of 0 and a polar surface area (PSA_2D) of 0 suggest that it has a balanced hydrophobic and hydrophilic profile, which may facilitate its interaction with both cell membranes and aqueous biological environments. This balance is important for optimizing the delivery and efficacy of the nanofluid in targeting *Plasmodium falciparum*.

In conclusion, the ADMET profile of the Au–Pt–Ag trimetallic nanofluids reveals a promising therapeutic potential with moderate solubility, manageable hepatotoxicity risks, and favorable absorption and plasma protein binding characteristics. While the low BBB permeability may limit its use in treating cerebral malaria, the overall profile suggests that these nanofluids could be effectively employed in the broader treatment of malaria. The results underscore the importance of further experimental validation, particularly regarding hepatotoxicity and CYP2D6 interactions, to ensure safety and efficacy in clinical applications.

Toxicity and carcinogenicity profile of Au–Pt–Ag trimetallic nanofluids: a detailed assessment

The comprehensive toxicity and carcinogenicity assessment (Table 9 and Fig. 11) of Au–Pt–Ag trimetallic nanofluids, as presented in Table 5, provides valuable insights into their safety profile. This evaluation utilizes TOPKAT (Toxicity Prediction by Komputer Assisted Technology) predictions across multiple species, including mice and rats, under various conditions to determine the potential risks associated with these nanofluids when used in therapeutic applications.

The TOPKAT predictions for female and male mice using the NTP (National Toxicology Program) model show a divergence in

carcinogenicity. The nanofluids are predicted to be non-carcinogenic in female mice, with a probability of 0.594359, and an enrichment score of 1.51032. However, in male mice, the prediction shifts to carcinogenicity, with a higher probability of 0.640877 and a significant enrichment score of 1.6291. This gender-based difference highlights the importance of considering sex-specific responses when evaluating the safety of nanomaterials.

For rats, the predictions follow a similar trend, with both male and female rats predicted to be at risk of carcinogenicity. Female rats have a probability of 0.540734 and an enrichment score of 1.18798, while male rats exhibit a slightly higher probability of 0.629217 with an enrichment score of 1.23648. These results suggest a potential risk of long-term carcinogenic effects, particularly in male subjects, underscoring the need for careful monitoring and further investigation in preclinical studies.

Additionally, the TOPKAT FDA predictions categorize the nanofluids as multi-carcinogens for both male and female mice and rats. This classification indicates that the nanofluids may possess multiple mechanisms or pathways that contribute to their carcinogenic potential. The single *vs.* multiple carcinogen predictions reinforce this, with multiple carcinogenic tendencies observed across the board, particularly in female subjects.

The TOPKAT Ames test prediction, which assesses mutagenic potential, indicates that the Au–Pt–Ag nanofluids are non-mutagenic with a probability of 0.714302 and an enrichment score of 1.27926. This finding is crucial as it suggests that, despite their potential carcinogenicity in certain contexts, the nanofluids do not directly induce genetic mutations—a key factor in evaluating the overall safety of the material.

Other significant toxicity predictions include the skin irritancy and sensitization assessments. The nanofluids are predicted to be mild irritants with a strong sensitization potential, which could lead to allergic reactions upon repeated exposure. The ocular irritancy predictions similarly indicate mild irritancy, which is crucial for applications where contact with sensitive tissues is a possibility.

The environmental toxicity predictions, such as the fathead minnow LC_{50} and daphnia EC_{50}, suggest that the nanofluids could pose a risk to aquatic life, with very low LC_{50} and EC_{50} values. This indicates high toxicity to these organisms, emphasizing the need for careful environmental impact assessments before large-scale use.

In conclusion, the TOPKAT-based toxicity and carcinogenicity assessment of Au–Pt–Ag trimetallic nanofluids reveals a complex safety profile. While the nanofluids exhibit non-mutagenic properties, their potential carcinogenicity, particularly in male subjects and under chronic exposure, warrants further investigation. The environmental toxicity findings also highlight the need for stringent environmental monitoring. These insights are critical for guiding the safe and effective development of AuPtAg nanofluids for biomedical applications, ensuring that potential risks are well-managed in clinical and environmental contexts.

Conclusion

This study demonstrates that Au–Pt–Ag trimetallic nanofluids exhibit significant antimalarial and antioxidant activity while maintaining low cytotoxicity, making them strong candidates for therapeutic development. Experimental validation, reinforced by statistical analysis (one-way ANOVA with Tukey's *post hoc* test, $p < 0.05$), confirmed their effectiveness and safety profile. The high therapeutic index (142.52) further highlights their selectivity and biocompatibility compared to conventional drugs.

Computational modeling, including Density Functional Theory (DFT), molecular docking, and molecular dynamics simulations, provided deeper insights into the electronic structure and biological interactions of these nanofluids. Strong binding affinities with *Plasmodium falciparum* proteins suggest potential as antimalarial agents, though their binding energies remain lower than some standard drugs. ADMET analysis also indicates favorable pharmacokinetic properties, including good intestinal absorption and low toxicity, reinforcing their suitability for further development.

Despite these promising findings, further research is essential to optimize formulation parameters, enhance bioavailability, and evaluate long-term safety. *In vivo* studies will be crucial to determine their efficacy in biological systems, and detailed mechanistic investigations are required to elucidate their precise mode of action at the molecular level.

Additionally, this study provides critical insights into the cytotoxic effects of Au–Pt–Ag nanofluids on human HepG2 cells, demonstrating their potential as a safer alternative to conventional antimalarial treatments. Comprehensive safety evaluations, including long-term cytotoxicity, biodistribution, and metabolism studies, will be necessary to ensure their viability for clinical applications.

These findings highlight the potential of nanotechnology-driven therapeutics for malaria and oxidative stress-related disorders, bridging the gap between theoretical predictions and experimental outcomes. With continued refinement, Au–Pt–Ag nanofluids could offer a novel, targeted approach to antimalarial and antioxidant therapies, contributing to the development of safer and more effective treatment strategies.

Data availability

The data that supports the findings of this study are available on request from corresponding author.

Author contributions

Amit Dubey: supervision, investigation, conceptualized, writing the original draft (*in silico* work, antimalarial and antioxidant), software (molecular docking, molecular dynamics, residue distance maps, DFT, MESP, and ADMET), visualization, methodology, writing – review & editing, data curation, validation and formal analysis. Manish Kumar: writing original draft (antimalarial, antioxidant and molecular dynamics), validation. Aisha Tufail: writing the original draft (*in silico* work),

visualization, validation. Abhay D. Bagul: writing review and editing, validation.

Conflicts of interest

The authors declare that they have no known competing financial interests or personal relationships that could have appeared to influence the work reported in this paper.

Acknowledgements

The author (MK) expresses gratitude to Prof. A. S. Singh, Principal of Iswar Saran Degree College, Prayagraj, for providing them with a state lab facility, which was crucial for their research work. They express their gratitude for Prof. Singh's support and commitment to academic excellence, highlighting his invaluable contribution to scientific knowledge and innovation.

References

1 World Health Organization, *World Malaria Report*, 2023, https://www.who.int/initiatives/sdg3-global-action-plan/progress-and-impact/progress-reports/2023.
2 E. A. Ashley, M. Dhorda, R. M. Fairhurst, C. Amaratunga, P. Lim, S. Suon, S. Sreng, J. M. Anderson, S. Mao, B. Sam and C. Sopha, Spread of artemisinin resistance in Plasmodium falciparum malaria, *N. Engl. J. Med.*, 2014, **371**, 411–423.
3 W. Cai, T. Gao, H. Hong and J. Sun, Applications of gold nanoparticles in cancer nanotechnology, *Nanotechnol., Sci. Appl.*, 2008, **19**, 17–32.
4 H. Rashidzadeh, S. J. Tabatabaei Rezaei, S. M. Adyani, M. Abazari, S. Rahamooz Haghighi, H. Abdollahi and A. Ramazani, Recent advances in targeting malaria with nanotechnology-based drug carriers, *Pharm. Dev. Technol.*, 2021, **26**, 807–823.
5 M. Rai, A. Yadav and P. D. Gupta, Silver nanoparticles as a potential anti-malarial agent, *Mol. Biotechnol.*, 2009, **42**, 167–173.
6 N. Yadav, A. K. Jaiswal, K. K. Dey, V. B. Yadav, G. Nath, A. K. Srivastava and R. R. Yadav, Trimetallic Au/Pt/Ag based nanofluid for enhanced antibacterial response, *Mater. Chem. Phys.*, 2018, **218**, 10–17.
7 N. Yadav, R. R. Yadav and K. K. Dey, Microwave assisted formation of trimetallic AuPtCu nanoparticles from bimetallic nano-islands: why it is a superior new age biocidal agent compared to monometallic & bimetallic nanoparticles, *J. Alloys Compd.*, 2022, **896**, 163073.
8 A. K. Maddheshiya, M. Kumar, A. Tufail, P. S. Yadav, Y. Deswal, N. Yadav, T. P. Yadav and A. Dubey, Synergistic Activity of Noble Trimetallic Nanofluids: Unveiling Unprecedented Antimicrobial Potential and Computational Insights, *ACS Appl. Bio Mater.*, 2024, **7**, 5906–5924.
9 K. H. Rieckmann, J. V. McNamara, H. Frischer, T. A. Stockert, P. E. Carson and R. D. Powell, Gametocytocidal and sporontocidal effects of primaquine and of sulfadiazine with pyrimethamine in a chloroquine-resistant strain of Plasmodium falciparum, *Bull. W. H. O.*, 1968, **38**(4), 625.
10 B. Kumar, J. Devi, A. Dubey, A. Tufail and S. Sharma, Exploring the antimalarial, antioxidant, anti-inflammatory activities of newly synthesized transition metal (II) complexes bearing thiosemicarbazone ligands: insights from molecular docking, DFT, MESP and ADMET studies, *Inorg. Chem. Commun.*, 2024, **159**, 111674.
11 M. R. Espíndola, F. D. Varotti, A. C. Aguiar, S. N. Andrade and E. M. Rocha, In vitro assessment for cytotoxicity screening of new antimalarial candidates, *Braz. J. Pharm. Sci.*, 2022, **58**, e18308.
12 M. Kumar, K. Pal, V. Pratap and J. K. Gour, Antileishmanial potential of different extracts of Curcuma longa rhizome against Leishmania donovani, *J. Sci. Res.*, 2022, **66**, 129–141.
13 A. Imraish, M. Zihlif, T. Abu Thiab, W. Al-Awaida, H. J. Al-Ameer, B. E. Abu-Irmaileh and A. Al-Hunaiti, Anti-Inflammatory and Antioxidant Effects of Rosmarinic Acid Trimetallic ($Cu_{0.5}Zn_{0.5}Fe_2O_4$) Nanoparticles, *Chem. Biodiversity*, 2024, **21**, e202301739.
14 M. Roney, A. Dubey, M. H. Nasir, A. M. Huq, A. Tufail, S. N. Tajuddin, N. B. Zamri and M. F. Mohd Aluwi, Computational evaluation of quinones of Nigella sativa L. as potential inhibitor of dengue virus NS5 methyltransferase, *J. Biomol. Struct. Dyn.*, 2024, **42**, 8701–8711.
15 J. Dundas, Z. Ouyang, J. Tseng, A. Binkowski, Y. Turpaz and J. Liang, CASTp: computed atlas of surface topography of proteins with structural and topographical mapping of functionally annotated residues, *Nucleic Acids Res.*, 2006, **34**(suppl_2), W116–W118.
16 W. Tian, C. Chen, X. Lei, J. Zhao and J. Liang, CASTp 3.0: computed atlas of surface topography of proteins, *Nucleic Acids Res.*, 2018, **46**(W1), W363–W367.
17 G. M. Morris, R. Huey, W. Lindstrom, M. F. Sanner, R. K. Belew, D. S. Goodsell and A. J. Olson, AutoDock4 and AutoDockTools4: automated docking with selective receptor flexibility, *J. Comput. Chem.*, 2009, **30**, 2785–2791.
18 A. Dubey, A. Facchiano, P. W. Ramteke and A. Marabotti, In silico approach to find chymase inhibitors among biogenic compounds, *Future Med. Chem.*, 2016, **8**, 841–851.
19 A. Dubey, A. Marabotti, P. W. Ramteke and A. Facchiano, Interaction of human chymase with ginkgolides, terpene trilactones of Ginkgo biloba investigated by molecular docking simulations, *Biochem. Biophys. Res. Commun.*, 2016, **473**, 449–454.
20 A. Dubey, M. M. Alawi, T. A. Alandijany, I. M. Alsaady, S. A. Altwaim, A. K. Sahoo, V. D. Dwivedi and E. I. Azhar, Exploration of microbially derived natural compounds against monkeypox virus as viral core cysteine proteinase inhibitors, *Viruses*, 2023, **15**, 251.
21 Y. Yiqing, Y. Yu, X. Li, J. Li, Y. Wu, J. Yu, J. Ge, Z. Huang, L. Jiang, Y. Rao and M. Yang, Target elucidation by cocrystal structures of NADH-ubiquinone oxidoreductase of Plasmodium falciparum (Pf NDH2) with small molecule to eliminate drug-resistant malaria, *J. Med. Chem.*, 2017, **60**, 1994–2005.

22 S. Bharadwaj, A. Dubey, N. K. Kamboj, A. K. Sahoo, S. G. Kang and U. Yadava, Drug repurposing for ligand-induced rearrangement of Sirt2 active site-based inhibitors via molecular modeling and quantum mechanics calculations, *Sci. Rep.*, 2021, **11**, 10169.

23 A. Dubey, S. Dotolo, P. W. Ramteke, A. Facchiano and A. Marabotti, Searching for chymase inhibitors among chamomile compounds using a computational-based approach, *Biomolecules*, 2018, **9**(1), 5.

24 P. K. Doharey, P. Verma, A. Dubey, S. K. Singh, M. Kumar, T. Tripathi, M. Alonazi, N. J. Siddiqi and B. Sharma, Biophysical and in-silico studies on the structure-function relationship of Brugia malayi protein disulfide isomerase, *J. Biomol. Struct. Dyn.*, 2024, **11**, 1533–1543.

25 S. Bharadwaj, A. Dubey, U. Yadava, S. K. Mishra, S. G. Kang and V. D. Dwivedi, Exploration of natural compounds with anti-SARS-CoV-2 activity via inhibition of SARS-CoV-2 Mpro, *Briefings Bioinf.*, 2021, **22**, 1361–1377.

26 D. Majumdar, A. Dubey, A. Tufail, D. Sutradhar and S. Roy, Synthesis, spectroscopic investigation, molecular docking, ADME/T toxicity predictions, and DFT study of two trendy ortho vanillin-based scaffolds, *Heliyon*, 2023, **9**(6), e16057.

27 D. Majumdar, J. E. Philip, A. Dubey, A. Tufail and S. Roy, Synthesis, spectroscopic findings, SEM/EDX, DFT, and single-crystal structure of Hg/Pb/Cu–SCN complexes: in silico ADME/T profiling and promising antibacterial activities, *Heliyon*, 2023, **9**(5), e16103.

28 M. Dalal, A. Dubey, A. Tufail, N. Antil, N. Sehrawat and S. Garg, Organyltellurium(IV) complexes incorporating Schiff base ligand derived from 2-hydroxy-1-naphthaldehyde: preparation, spectroscopic investigations, antimicrobial, antioxidant activities, DFT, MESP, NBO, molecular docking and ADMET evaluation, *J. Mol. Struct.*, 2023, **1287**, 135590.

29 M. J. Frisch, *Gaussian 09, Revision d. 01*, Gaussian Inc., Wallingford CT, 2009, p. 201.

30 B. Kumar, J. Devi, A. Dubey, A. Tufail and N. Antil, Biological and computational investigation of transition metal(II) complexes of 2-phenoxyaniline-based ligands, *Future Med. Chem.*, 2023, **15**, 1919–1942.

31 B. Kumar, J. Devi, A. Dubey, A. Tufail and B. Taxak, Investigation of antituberculosis, antimicrobial, anti-inflammatory efficacies of newly synthesized transition metal(II) complexes of hydrazone ligands: structural elucidation and theoretical studies, *Sci. Rep.*, 2023, **13**(1), 15906.

32 N. Dawar, J. Devi, B. Kumar and A. Dubey, Synthesis, characterization, pharmacological screening, molecular docking, DFT, MESP, ADMET studies of transition metal(II) chelates of bidentate Schiff base ligand, *Inorg. Chem. Commun.*, 2023, **151**, 110567.

33 B. Kumar, J. Devi, A. Dubey, A. Tufail and N. Antil, Biological and computational investigation of transition metal(II) complexes of 2-phenoxyaniline-based ligands, *Future Med. Chem.*, 2023, **15**, 1919–1942.

34 D. E. Pires, T. L. Blundell and D. B. Ascher, pkCSM: predicting small-molecule pharmacokinetic and toxicity properties using graph-based signatures, *J. Med. Chem.*, 2015, **58**, 4066–4072.

35 A. Dubey, V. Singh, P. K. Doharey, M. P. Sk, S. K. Samanta, V. Nema, B. Sharma, P. K. Varadwaj and A. K. Sahoo, Modulating catalytic activity of human topoisomerase II α enzyme by fluorescent gold nanoclusters, *Int. J. Biol. Macromol.*, 2021, **170**, 523–531.

36 S. Varela-Aramburu, C. Ghosh, F. Goerdeler, P. Priegue, O. Moscovitz and P. H. Seeberger, Targeting and inhibiting Plasmodium falciparum using ultra-small gold nanoparticles, *ACS Appl. Mater. Interfaces*, 2020, **12**, 43380–43387.